Use of dapsone (dap) to derive a novel series of diamines and their ensuing metallomacrocyclic complexes: Synthesis, characterization, DFT and cytotoxic study against Hep G2 and C6 cancer cell lines

Abstract

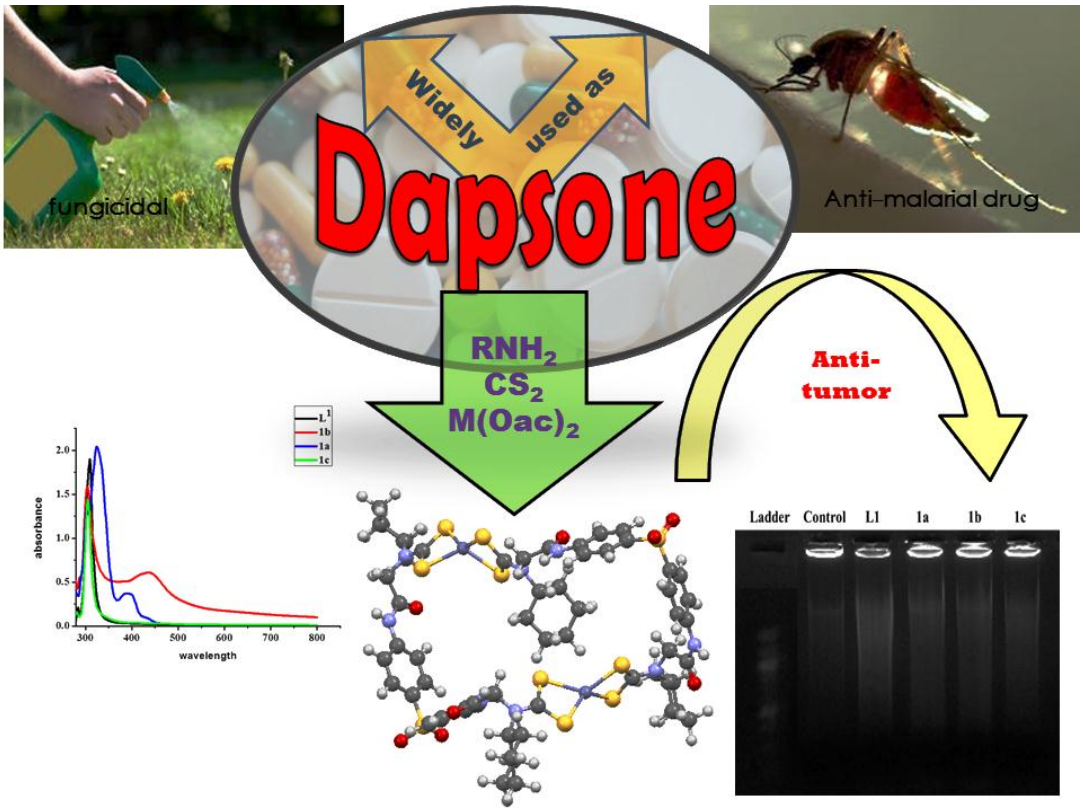

Interesting biological profile of dapsone (dap) has encouraged us to derivatize it further into a novel series of diamines 4,4'-bis(2-(alkylamino) acetamido) diphenylsulfone $\mathbf{L^1}$-$\mathbf{L^3}$ and their ensuing metallomacrocyclic complexes of the type [M_2-μ^2-bis-{(κ^2*S*,*S*-$S_2CN(R)CH_2CONHC_6H_4)_2SO_2$}] {R = *Cy*, M = Ni^{II} **1a**, Cu^{II} **1b,** Zn^{II} **1c**; R = ^{i}*Pr*, M = Ni^{II} **2a**, Cu^{II} **2b,** Zn^{II} **2c**; R = ^{n}*Bu*, M = Ni^{II} **3a**, Cu^{II} **3b,** Zn^{II} **3c**}. These compounds were characterized by standard spectroscopic methods. A DFT

level calculation has been performed on selected compounds. *In vitro* cytotoxic activity against Hep G2 (hepatoma) and C6 (Glioblastoma) cell lines suggests specificity of these compounds for cancer cells over normal liver cells. Interestingly, complex 2c holding zinc(II) and *N*-^{i}Pr substituents shows nearly 3 fold better cytotoxic activity against both Hep G2 (8.47±0.016 µg/mL) and C6 (4.3±0.019 µg/mL) cell lines, compared to the reference drug Cisplatin. The morphological changes and moderate to heavy DNA laddering clearly demonstrate the induction of apoptotic cell death, required for major chemical therapeutic implications.

2.1 Introduction

The interest in dap has been continued since its inception in clinical practice [1] as antibiotic in the late 1940s. Reports suggest that it is active against various species of Pneumocystis, Plasmodia, Toxoplasma, and Mycobacteria and used in both cancer and human immunodeficiency virus (HIV) patients. [2] A combination of dap and chlorproguanil which is commercially known as Lapdap act synergistically against malaria [3] however, this drug reportedly causes haemolysis in patients with G6PD deficiency.[4] It is slowly absorbed after oral administration with a mean absorption half-life of 1.1 hours that reaches peak serum or plasma concentrations in about 2–6 hours with considerable variations.[5] Absolute oral bioavailability is calculated to exceed 85% [6] where 70–90% of dap is bound to plasma protein and distributed throughout the tissues, crosses the placenta and is excreted in breast milk, saliva, feces and urine as 4,4'-diaminodiphenyl sulfone hydroxylamine.[7] It can also be bio-transformed to a nontoxic metabolite, the monoacetyl dapsone (MADDS) by arylamine NAT.[8, 9]

Besides, the success of a wide range of natural product bearing a macrocyclic motif in clinical use with a high degree of potency as well as selectivity [10] has inspired synthetic chemists to explore a broader use of macrocyclic scaffolds in medicinal chemistry. The past two decades have witnessed that the combination of metal with di-or-oligofunctional ligands allows the creation of a large number of metallosupramolecular architectures having either macrocyclic, cage-like or polymeric structures.[11] A series of different applications such as selective molecular and ion recognition, separation, storage,

transport and catalysis are envisioned for these systems.[12] A variety of guest substrates have been encapsulated and stabilized by metallomacrocyclic structures as well as chemical reactions being catalyzed, within these "micro reactor" cores.[13] Recently our group has successfully utilized 4,4'-diaminodiphenyl ether to derive a number of bisimines, diamines, bimetallic metallomacrocyclic structures and systematically investigated these derivatives from medicinal perspectives.[14a-14c]

In the light of these observations, it was pertinent to select dap as a lead compound to derive 4,4'-bis(2-(cyclohexylamino)acetamido)diphenylsulfone (L^1), 4,4'-bis(2-(isopropylamino)acetamido)diphenylsulfone (L^2), 4,4'-bis(2-(n-butylamino)acetamido)-diphenylsulfone (L^3) and their ensuing metallomacrocyclic dithiocarbamate complexes to explore their possible cytotoxic abilities against human cancer cell lines viz. Hep G2 (Hepatoma) and C6 (Glioblastoma). Hepatocytes have the ability to metabolize, detoxify and inactivate exogenous compounds such as drugs and also endogenous compounds like steroids and thus liver is a major site of synthesis and metabolism of major biomolecules like proteins and carbohydrates. In particular, Hep G2 (hepatoblastoma) cell line is commonly used for xenobiotic metabolic studies as it maintains many specialized functions of liver cells. Moreover, neuronal cells behave differently compared to other cells of the body and this inconsistency may be attributed to the reason that the brain is separated by a strong blood brain barrier which principally decides what molecules to pass and what to block.[14d] Thus Hepatoma Hep G2 and Glioblastoma C6 cell lines were selected for the evaluation of cytotoxic properties of these newly synthesized compounds.

Herein, we report on the synthesis, spectroscopic characterization, thermal analysis, electrochemical study, DFT calculations and biological reactivity of a number of derivatives of dap viz. L^1-L^3 and [M^{II}_2-μ^2-bis-{(κ^2*S*,*S*-$S_2CN(R)C_6H_4)_2SO_2$}] {R = *Cy*; M = Ni^{II} **1a**, Cu^{II} **1b**, Zn^{II} **1c**; R = ^{i}*Pr*; M = Ni^{II} **2a**, Cu^{II} **2b**, Zn^{II} **2c**; R = ^{n}*Bu*; M = Ni^{II} **3a**, Cu^{II} **3b**, Zn^{II} **3c**}. The presence of dapsone moieties along with biologically relevant amide groups and transition metal ions in the macrocyclic framework of **1a-1c, 2a-2c, 3a-3c** would facilitate the interaction of these molecules with biomolecules through potential donor-acceptor interactions i.e. non-conventional hydrogen bonding interactions.

2.2. Experimental Section

2.2.1. Materials and Instrumentations

Metal acetates were purchased from Merck, dapsone was purchased from National Chemicals and all solvents such as chloroacetylchloride, chloroform, acetonitrile, absolute alcohol, n-hexane were purchased from Chemlab. All other solvents and reagents were of AR grade and have been used without further purification.The lead precursor 4,4'-bis(2-chloroacetamido)diphenylsulfone (**Dac)** was synthesized from dapsone by reacting chloroacetyl chloride under mild basic condition, following a modified literature procedure. Reactions and manipulations were performed under an inert atmosphere. Melting points were recorded in open capillaries and uncorrected. Thin Layer Chromatography was performed on Merck 60 F254 aluminium coated plates. ESI-MS spectra were obtained on AB SCIEX 3200 Q TRAP LCMS instrument whereas high resolution mass spectrometric analysis (HRMS) was performed on Waters Micromass Q-Tof micro™ mass spectrometer equipped with electrospray ionisation source and time-of-fight (TOF) analyzer Capillary and voltage was set at 2.5KV. FT-IR (KBr pellets) spectra were recorded in the 4000-400 cm^{-1} range using a Perkin-Elmer FT-IR spectrometer. The NMR spectra were obtained on a Bruker AV-III 400 MHz spectrometer in $CDCl_3$/d^6-DMSO solvents as per the solubility and chemical shifts are reported in parts per million (ppm). UV-visible absorption spectra were recorded on a Perkin Elmer Lambda 35 UV-visible spectrophotometer. Fluorescence was recorded on JASCO make spectrofluorometer model FP-6300. TGA/DTA plots were obtained using SII TG/DTA 6300 in flowing N_2 with a heating rate of 10°C min^{-1}. Electrochemical measurements were performed on a CH Instruments 600C potentiostat, using a Pt disk as the working electrode, Ag/AgCl as the reference electrode and a Pt wire as the counter electrode. Voltammograms were recorded by using anhydrous solutions of the metal complexes in CH_2Cl_2 (1.0 mm) containing tetra-n-butylammoniumhexafluoro phosphate (0.1M) as supporting electrolyte.

2.2.2. General method of preparation of secondary diamine precursors L^1-L^3

4,4'-bis(2-chloroacetamido)diphenylsulfone (DAc)

To a 50 mL chloform solution containing 1 equivalent (0.5 g; 2.01 mmol) of dapsone, 3 equivalent (0.507 g; 6.04 mmol) of$NaHCO_3$, was added 2.5 equivalents (0.568 g; 5.03mmol) of chloroacetyl chloride drop wise over a period of 40 minutes at 0 ºC. The reaction mixture was allowed to stir for 3hrs at room temperature and reaction progress was monitored by TLCs. The residue was filtered over glass sintered crucible, washed with 3 × 5 mL of 5% of $NaHCO_3$, 3 × 5 mL of distilled water followed by hexane. Finally the residue was dried under high vaccum to yield the white product which was taken for the analysis.

Yield: 0.624 g, 77%. m.p. 232°C. ^{1}H NMR (500 MHz, $CDCl_3$): δ (ppm) 11.187 (s, 2H, NH); 8.335 (d, 4H, Ph); 7.985(dd, 4H, Ph); 4.242(s, 4H, CH_2). FT IR (cm^{-1}, KBr pellet): 3496 w, 3266 s, 3197 s, 8127s, 3078m, 2891w, 1678s, 1614s, 1592s, 1546s, 1436m, 1404s, 1338s, 1304s, 1256s, 1182m, 1153s, 1107s, 1073m, 976m, 839s, 752s, 669s, 660s, 601s, 540m.

4,4'-bis(2-(alkylamino)acetamido)diphenylsulfone L^1-L^3

To a solution of absolute ethanol containing 4,4'-bis(2-chloroacetamido) diphenylsulfone (802 mg, 2mmol), was added excess amount of cyclohexyl amine (891.9 mg, 9mmol), isopropyl amine (531.9 mg, 9mmol) or n-butyl amine (657.9 mg 9 mmol) in the presence of Et_3N and the reaction mixture was refluxed for 7 hrs. The reaction was monitored by TLC. The reaction mixture was cooled at room temperature and then it was poured onto ice. The residue obtained was isolated by filtration and washed further with cold water, followed by n-hexane and diethyl ether to yield diamines **L^1-L^3** in good yields. These were stored under a nitrogen atmosphere and samples were taken for analysis.

4,4'-bis(2-(cyclohexylamino)acetamido)diphenylsulfone (L^1): MW: 526, Yield: 999.4 mg, 95%. m.p. 190°C dec. ES-MS: 527.1 (M+H). Infrared spectrum (KBr disc, cm^{-1}): 3285.03(-NH)(w), 3180.75(-CH)(w), 3102.78(w), 3044.05, 2928.28(s), 2852.88(s), 2595.14(w), 1918.79(w), 1703 (C=O)(s), 1591.71(s), 1448.36(m), 1403.92(s), 1318.89(s), 1258.69(m), 1180.55(m), 1154.40(s), 1107.55(s), 1074.09(w), 960.87(w),

893.37(w), 840.50 (s), 690.60(w), 632.55(w), 553.00(w), 464.41(w). ^{1}HNMR (400 MHz, DMSO-d_6): δ (ppm) 7.87-7.82 (m, 8H, Ph); 3.35 (s, 4H, NC*H*$_2$CO); 2.31 (m, 2H,-NC*H* of Cy); 1.78 (s, br, 2H, NH); 1.756-1.18 (m, 20H, cyclohexyl). ^{13}C NMR (400 MHz, DMSO-d_6): δ (ppm) δ 172.2 (C=O), 143.4, 135.7, 128.9, 119.6 (C of Ph), 56.6, (C of CH_2), 50.7 (C of –N*C*H), 33.2, 26.1, 24.8 (C of cyclohexyl).

4,4'-bis(2-(isopropylamino)acetamido)diphenylsulfone (L^2): MW: 446, Yield: 767.1 mg, 86%. m.p. 170°C dec. ES-MS: 447.0 (M+H). Infrared spectrum (KBr disc, cm^{-1}): 3369.18(N-H)(w), 3280.80(w), 3181.01(w), 3104.00(C-H aromatic)(w), 2967.29(C-H aliphatic)(m), 1702.20(C=O)(vs), 1592.66(C=C)(vs), 1520.55(vs), 1475.71(w), 1403.70(s), 1360.62(m), 1318.80(m), 1261.95(s), 1183.45(m), 1154.84(vs), 1108.43(s), 1011.48(w), 957.86(w), 836.14(s), 748.77(w), 717.28(w), 691.55(m), 604.41(w), 580.56(m), 560.72(m). ^{1}H NMR (400 MHz, DMSO-d_6): δ (ppm) 7.87-7.82 (m, 8H,Ph); 3.29 (s,4H, NC*H*$_2$CO); 1.734 (s, br, 2H, NH); 2.70 (m,2H,-NC*H* of ^{i}Pr); 0.98-0.96 (d, 12H, -CH_3). ^{1}H NMR (400 MHz, $CDCl_3$): δ (ppm) 9.755 (s, 2H, CON*H*), 7.905 (d, 4H, J=8.8 Hz, phenyl Ca,a'), 7.742 (d, 4H, J=8.8 Hz, phenyl Cb,b'), 3.383 (s, 4H, NC*H*$_2$CO); 2.872-2.841 (m, 2H, -CH of ^{i}Pr); 1.630 (s, 2H, NH), 1.123 (d, 12H, -CH_3).^{13}C NMR (400 MHz, $CDCl_3$): δ (ppm) 171.1 (C=O), 141.8, 136.4, 128.8, 119.1 (C of Ph), 50.8 (CH_2), 49.9 (N*C*H) , 23.0 (CH_3).

4,4'-bis(2-(n-butylamino)acetamido)diphenylsulfone (L^3): MW: 474,Yield: 872.1 mg, 92%. m.p. 118°C dec. ES-MS: 475.1 (M+H). Infrared spectrum (KBr disc, cm^{-1}): 3548.82(s), 3184.78(w), 3104.55(C-H aromatic)(w), 3054.60(C-H aliphatic)(w), 2959.48(w), 2928.59(w), 2862.68(w), 1772.02(m), 1708.29(C=O)(m), 1591.37(C=C)(vs), 1524.09(vs), 1402.48(s), 1315.25(s), 1263.49(m), 1195.47(m), 1155.29(vs), 1106.93(s), 1073.49(w), 1008.27(w), 836.80(m), 728.27(m), 688.64(m), 609.52(m), 573.28(m), 531.05(w). ^{1}H NMR (400 MHz, DMSO-d_6): δ (ppm) 7.87-7.81 (m, 8H, Ph); 3.28 (s, 4H, NC*H*$_2$CO); 1.390 (merged with ^{n}Bu, NH); 1.41-1.26 (m,18H, $CH_2CH_2CH_2CH_3$). ^{13}C NMR (400 MHz, DMSO-d_6): δ (ppm) 170.7 (C=O), 141.9, 136.4, 128.8, 119.1 (C of Ph), 52.9 (N*C*H$_2$CO), 50.0 (N*C*H$_2$), 32.1, 30.9, 20.2, 13.9 (Bu).

2.2.3. General Synthetic procedure for metallomacrocyclic dithiocarbamate complexes 1a-1c, 2a-2c, 3a-3c

To a acetonitrile solution of 1 equivalent of respective diamine precursor $\mathbf{L^1}$ (0.263 g, 0.5mmol),$\mathbf{L^2}$ (0.223g, 0.5mmol) or $\mathbf{L^3}$ (0.237g, 0.5mmol), an excess amount of NaOH (~3 equivalent; ~ 0.060 g) and carbon disulfide (~10 equivalent; ~ 0.5 ml) were added with vigorous stirring. The mixture was stirred further for 12 h at room temperature. A change in color from colorless to pale yellow was observed during the progress of a reaction. To this reaction mixture, $Ni^{II}(C_2H_3O_2)_2.4H_2O$ (136 mg, 0.55 mmol), Cu(OAc)2.H2O (0.111 g, 0.55 mmol)or $Zn^{II}(C_2H_3O_2)_2.2H_2O$ (121 mg, 0.55mmol), dissolved in a minimum amount of distilled water, was added with rigorous stirring and the reaction was allowed to continue for 8 h at room temperature. The reaction mixture was dried under vacuum and the residue was washed several times with distilled water, followed by n-hexane and diethyl ether. A free flowing powder obtained was dried under vacuum to yield the corresponding products **1a-1c, 2a-2c, 3a-3c**.

[Ni_2-μ^2-bis-{(κ^2*S,S*-$S_2CN(Cy)CH_2CONHC_6H_4)_2SO_2$}] (1a). Green; MW: 1471, Yield: *ca* 412 mg, 56%; m.p. >260 °C dec. ES-MS: 1510.6 (M+K). Infrared spectrum (KBr disc, cm^{-1}): 2935.48w, 2855.98w, 1763.80w, 1690.01s, 1678.92s, 1590.54s, 1522.30m, 1474.97m, 1401.48s, 1375.57m, 1312.88m, 1243.98m, 1151.48s, 1105.88m, 970.20w, 838.24m, 724.59w, 603.75w, 418.79w. ^{1}H NMR (400 MHz, DMSO-d6): δ (ppm) 10.637 (br s, CON*H*), 7.816-7.730 (braromatic C*H*), 4.38-4.286 (br, NCH_2CO), 3.50 (merged with solvent signal, C*H* of *Cy*), 1.680 (br s, CH_2 of *Cy*), 1.440 (br, s, CH_2 of *Cy*), 1.219 (br, s, CH_2 of *Cy*), 1.095 (br, s, CH_2 of *Cy*). ^{13}C NMR (400 MHz, DMSO-d6): δ (ppm) 207.5 **(-$N^{13}CS_2$)**, 165.5, (*C*=O) 143.3 (*C*-N), 129.0, 119.5, 113.6, (*C* of Ph), 59.3, (N*C*H_2CO) 48.3, (*C*Hof*Cy*), 29.2, 25.3, 24.8 (*C* of cyclohexyl).

[Cu_2-μ^2-bis-{(κ^2*S,S*-$S_2CN(Cy)CH_2CONHC_6H_4)_2SO_2$}] (1b).Brown; MW: 1481, Yield: *ca*385 mg, 52 %; m.p. 228 °C dec. ES-MS: 1488.5 (M+Li). Infrared spectrum (KBr disc, cm^{-1}): 3578.10w, 2934.44m, 2854.42w, 2485.66w, 1696.56s, 1590.42s, 1529.87s, 1452.00m, 1400.15s, 1311.89m, 1242.92m, 1105.67m, 1008.93m, 968.51w, 890.83w, 838.58m, 771.96w, 723.29(w), 667.13w, 605.91m, 551.96w, 410.35m.

[Zn_2-μ^2-bis-{(κ^2S,S-$S_2CN(Cy)CH_2CONHC_6H_4)_2SO_2$}] (1c). Pale Yellow; MW: 1484,Yield: *ca*438 mg, 59%; m.p. 214 °C dec. ES-MS: 1507.5 (M+Na). Infrared spectrum (KBr disc, cm^{-1}): 3456.67w, 2979.51w, 2929.11m, 2852.62w, 2656.62w, 1797.56w, 1702.58m, 1677.66w, 1589.57s, 1524.66s, 1449.08m, 1401.80m, 1319.81m, 1259.39w, 1230.88w, 1150.94s, 1105.77s, 1072.52w, 1009.75m, 967.80w, 890.68w, 841.62m, 723.51w, 665.98w, 605.81m, 581.17w, 547.66w, 533.62w, 475.24w. ^{1}H NMR (400 MHz, DMSO-d_6): δ (ppm) 10.52 (s, 4H, -CON*H*); 7.89-7.48 (m, 16H, Ph); 4.58 (s, 8H, NCH_2CO); 3.362 (merged with solvent signal, C*H* of *Cy*), 1.89-1.22 (m, 20H, CH_2 of *Cy*).^{13}C NMR (400 MHz, DMSO-d6): δ (ppm) 206.2 **(-N^{13}CS_2)**, 171.9, 166.8 (*C*=O), 143.8, 143.3, 135.8, 135.5 (*C*-N), 128.9, 128.9, 119.6, 119.3, 113.5 (*C* of Ph), 64.1, 56.7 (N*C*H_2CO), 52.0, 50.3 (*C*Hof*Cy*)), 32.8, 29.9, 26.0, 25.6, 25.0, 24.7 (*C* of cycloheyl).

[Ni_2-μ^2-bis-{(κ^2S,S-$S_2CN(^iPr)CH_2CONHC_6H_4)_2SO_2$}] (2a). Green; MW: 1311, Yield: *ca*275 mg, 42%; m.p. 287 °C dec. ES-MS: 1312.7 (M+H). Infrared spectrum (KBr disc, cm^{-1}): 3187.16w, 3108.51w, 3055.56w, 2975.70m, 2931.84w, 1704.36s, 1591.41vs, 1534.06vs, 1475.00vs, 1403.52s, 1367.67w, 1311.51s, 1254.77s, 1175.11s, 1152.01vs, 1106.45s, 1072.28s, 1011.23m, 970.20m, 838.39m, 725.14m, 638.71s, 461.70w. ^{1}H NMR (400 MHz, DMSO-d6): δ (ppm) 10.637 (br s, CON*H*), 7.816-7.730 (br, aromatic C*H*), 4.380 (br, NCH_2CO), 3.5 (merged with solvent signal, C*H* of ^iPr), 1.680, 1.440, 1.219 (br s, CH_3 of ^iPr). ^{13}C NMR (400 MHz, DMSO-d6): δ (ppm) 207.0 **(-N^{13}CS_2)**, 165.5 (*C*=O); 143.3 (*C*-N), 135.8, 129.0 119.6 (*C* of Ph), 51.4 (N*C*H_2CO), 47.5 (*C*H of ^iPr), 19.3 (*C*H_3 of ^iPr).

[Cu_2-μ^2-bis-{(κ^2S,S-$S_2CN(^iPr)CH_2CONHC_6H_4)_2SO_2$}] (2b). Brown; MW: 1320,Yield: *ca*304 mg, 46%; m.p. 227 °C dec. Infrared spectrum (KBr disc, cm^{-1}): 3261.22w, 3186.20w, 3106.64w, 2976.93m, 2934.23w, 1772.20w, 1740.70w, 1703.55s, 1591.17vs, 1537.97s, 1496.07m, 1467.94s, 1403.68s, 1367.74w, 1312.60vs, 1256.00s, 1179.01m, 1152.14s, 1106.55s, 1071.54s, 1010.74w, 968.25m, 839.13s, 723.67s, 636.00m, 622.52m, 417.73w.

[Zn_2-μ^2-bis-{(κ^2S,S-$S_2CN(^iPr)CH_2CONHC_6H_4)_2SO_2$}] (2c). Pale Yellow; MW: 1324,Yield: *ca* 344 mg, 52 %; m.p. 232 °C dec. ES-MS: 1325.6 (M+H). Infrared spectrum (KBr disc, cm^{-1}): 3282.38w, 3186.27w, 3110.65w, 2976.94m, 2930.61w, 1692.94s, 1591.69vs, 1534.67vs, 1462.56s, 1403.06s, 1364.06s, 1315.02s, 1253.60(s), 1177.12m, 1150.97s, 1107.34s, 1073.24s, 1005.06m, 968.39m, 837.63s, 723.67s, 637.85s, 568.42m, 417.45w.^{1}H NMR (400 MHz, DMSO-d6): δ (ppm) 10.49 (br s, CON*H*); 7.848-7.742 (m, aromatic C*H*); 4.544 (s, NCH_2CO); 3.52 (s, C*H* of ^iPr); 1.16(br, s,CH_3). ^{13}C NMR (400 MHz, DMSO-d6): δ (ppm) 205.9 **(-N^{13}CS_2)**, 166.8 (*C*=O); 143.8, 135.5, 130.5 (*C*-N); 128.9, 119.3, 113.4 (*C* of Ph), 56.1 (N*C*H_2CO), 51.1 (*C*H of ^iPr), 19.9, 19.5 (*C*H_3 of ^iPr).

[Ni_2-μ^2-bis-{(κ^2S,S-$S_2CN(^nBu)CH_2CONHC_6H_4)_2SO_2$}] (3a). Dark Green; MW: 1367, Yield: *ca*424 mg, 62 %; m.p. 250 °C dec. HRMS: 1387.0651 (M+Na). Infrared spectrum (KBr disc, cm^{-1}): 3328.92w, 3053.14w, 2960.33w, 2869.63w, 1700.67s, 1591.25vs, 1495.76s, 1434.98w, 1402.70m, 1313.64s, 1227.42m, 1180.02w, 1151.32s, 1106.57s, 1012.11w, 837.48m, 723.22m. ^{1}H NMR (400 MHz, DMSO-d6): δ (ppm) 10.678 (br s, CON*H*), 7.858-7.746 (br, aromatic C*H*); 4.449 (br s, NCH_2CO), 3.564 (br m, -NCH_2 of ^nBu), 1.540, 1.243 (br s, CH_2 of ^nBu); 0.857 (br, s, CH_3 of ^nBu).^{13}C NMR (400 MHz, DMSO-d6): δ (ppm) 207.4 **(-N^{13}CS_2)**, 165.3 (*C*=O), 143.3, 136.0 (*C*-N); 129.0, 119.6 (($C_{a,a',b,b'}$ of Ph); 52.0, (N*C*H_2CO) 51.2, (N*C*H_2 of ^nBu) 28.8, 19.7, (*C*H_2 of ^nBu); 14.0 (*C*H_3 of ^nBu).

[Cu_2-μ^2-bis-{(κ^2S,S-$S_2CN(^nBu)CH_2CONHC_6H_4)_2SO_2$}] (3b). Brown; MW: 1376,Yield: *ca* 385 mg, 56%; m.p. 225 °C dec. HRMS: 1375.0732 (M+H). Infrared spectrum (KBr disc, cm^{-1}): 3271.94w, 3185.82w, 3107.00w, 2960.82m, 2870.66m, 2361.59w, 1758.58m, 1692.93w, 1653.59w, 541.11vs, 1494.62s, 1432.27w. 1403.19vs, 1365.17m, 1314.73vs, 1255.85m, 1225.95m, 1151.15vs, 1106.57vs, 1073.12m, 1010.84m, 936.45w, 839.19s, 723.04m, 697.40w, 657.17w, 549.45w, 471.81w, 429.76m.

[Zn_2-μ^2-bis-{(κ^2S,S-$S_2CN(^nBu)CH_2CONHC_6H_4)_2SO_2$}](3c). Light orange; MW: 1380,Yield: *ca* 407 mg, 59 %; m.p. >220 °C dec. HRMS: 1399.0540 (M+Na). Infrared

spectrum (KBr disc, cm^{-1}): 3539.64w, 3279.83w, 3185.18w, 2959.78w, 1591.44vs, 1534.34s, 1491.87m, 1401.72s, 1369.02m, 1315.19m, 1254.80w, 1180.49w, 1151.13s, 1107.26m, 1071.63w, 1007.95w, 836.92m, 722.67w. ^{1}H NMR (400 MHz, DMSO-d6): δ (ppm) 10.53 (br s, CON*H*); 7.86 (d, J=8.4 Hz, aromatic C*H*), 7.75 (d,J=8.4 Hz, aromatic C*H*);4.68 (br s, NCH_2CO); 3.83 (br m, NCH_2); 1.66 (br,CH_2 of ^{n}*Bu*); 1.28 (br, CH_2 of ^{n}*Bu*); 0.89 (br, CH_3 of ^{n}*Bu*). ^{13}C NMR (400 MHz, DMSO-d6): δ (ppm) 206.7 **(-N^{13}CS_2)**, 166.6 (*C*=O), 143.7, 135.6 (*C*-N); 128.9, 119.4 (($C_{a,a',b,b'}$ of Ph); 57.6, 56.8 (NCH_2CO), 31.4, 31.1 (NCH_2 of ^{n}*Bu*); 28.8, 19.9 (CH_2 of ^{n}*Bu*); 14.1 (CH_3 of ^{n}*Bu*).

2.2.4. In vitro cytotoxic study

2.2.4.1. Cell line and culture

The human cancer cell lines HEP G2 (Hepatoma) and C6 (Glioblastoma) were procured from the National Centre for Cell Science, Pune whereas Dubecoo's Modified Eagle's Medium (DMEM), Fetal Bovine Serum (FBS) and antimycotic–antibiotic solution were procured from Gibco, Invitrogen and Cisplatin from Sigma Aldrich. The human cell line HEP G2 and C6 were maintained in DMEM with 10% FBS in humidified atmosphere supplied with 5% CO_2 at 37 °C. Both the cell lines were utilized to examine the cytotoxic activity of testing compound at varying concentration.

2.2.4.2. MTT assay for cell viability/ proliferation

The MTT assay was used to determine cell growth inhibition with some modifications. All the compounds viz. **Dap, Dac**, **L^1, L^2, L^3** and their ensuing transition metal dithiocarbamate complexes **1a-1c, 2a-2c, 3a-3c** were dissolved in DMSO and then diluted with water. The content of DMSO in each sample was 5%. Cells were seeded in 96-well plates at a density of 1×10^3 cells per well and incubated for 24hrs after which cells were treated with different concentrations of compounds reported in this paper for 24hrs. Under the similar experimental conditions cisplatin was also screened against both the cell lines. Finally the media were removed and the culture was incubated with 10 µL of media containing 5 mg/ml stock solution of MTT in PBS 4 h at 37°C in 5% CO_2 incubator. The resultant formazan crystal formed by metabolically viable cells was dissolved by adding DMSO. The optical density was measured at 540nm by an ELISA

reader (BIOTEK ELX800 Universal Microplate Reader). The number of viable cells was proportional to the extent of formazan production.

2.2.4.3. Statistical Analysis for Determination of IC_{50}

Data obtained was analyzed in Prism/ OriginPro 8 for standard error and probit analysis. The percent cytotoxicity index (% CI) was calculated as follows:

% CI= [1− (OD of treated cells/ ODof control cells)] × 100 %

where, CI= cytotoxicity index, OD= optical density.

A plot of % CI versus concentration was obtained from the experimental data for each set of experiments. The values of IC_{50} (50% growth inhibition of cell) were determined from the graph.

2.2.4.4. DNA ladder assay

Hep G2 cells (3×10^6) were exposed to the IC50 concentration of the compounds. Cells were centrifuged and then washed with PBS, and the pellet was lysed with 400 µL hypotonic buffer solution [containing 10 mM of tris (pH 7.5), 1 mM of EDTA and 0.2% triton X-100] for 15 min at room temperature, and then centrifuged at 13000 RPM for 15 min. 350 µL of the supernatant was again lysed in 106 µL of second lysis buffer [150 mMNaCl, 10 mMTrisHCl (pH 8.0), 40 mM EDTA, 1% SDS and 0.2 mg/ml of proteinase K, at final concentration] for 4 h at 37^0C. The DNA was extracted with phenol/chloroform/isoamyl alcohol (25:25:1 v/v/v), and the pellet, thus obtained was washed with ethanol and re-suspended for RNAase digestion in 15 µL of 10 mMTris, 1 mM of EDTA (pH 8.5), and 50 µg/mL of RNAase for 1 h at 37^0C. The fragmented DNA was quantified on 2% agarose gel electrophoresis. Finally, electrophoresis of the obtained DNA was carried out on a 1% agarose gel containing ethidium bromide at 50V for 1-2hrs. The gel was examined and photographed under the BioRadGelDoc system to visualize intra-nucleosomal DNA fragmentation (laddering).[13]

2.3. Result and Discussion

2.3.1. Syntheses and characterization

In continuation to our ongoing research interest [14] and absolute oral bioavailability of

dap in dogs and humans, [15] we have selected dap as a lead compound to derive a number of diamines and their transition metal dithiocarbamate complexes towards our search for a convincing cytotoxic agent. The α-chloroamide *viz* 4,4'-bis(2-chloroacetamido)diphenylsulfone (**Dac**) was prepared according to the Scheme 1. The formulation and purity of **Dac** was confirmed by NMR and IR spectroscopy. The ^{1}H NMR spectra this precursor showed signals at 11.187, 8.335-7.985 and 4.242 ppm with proper splitting patterns due to amide, aromatic and α-methylene protons respectively. **Dac** was used for the synthesis of diamine precursors **L^{1}-L^{3}**.

Three secondary diamino 4,4'-bis(2-(alkylamino)acetamido)diphenylsulfone (**L^{1}-L^{3}**) precursors were synthesized in >86 % yields by the nucleophilic substitution of α-chlorosubstituent of 4,4'-bis(2-chloroacetamido)diphenylsulfone (**Dac**) with a number of primary amines (Scheme 2) and these were characterized suitably by standard spectroscopic methods.

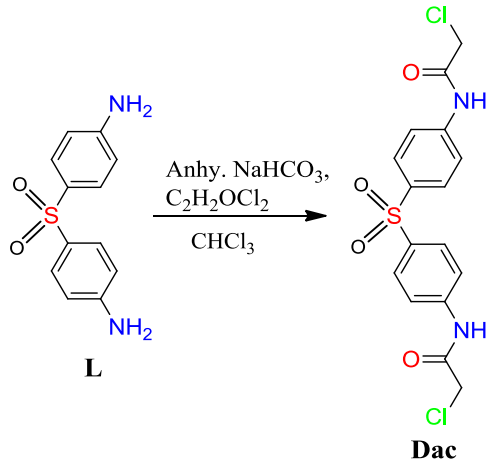

Scheme 1: Reaction scheme for 4,4'-bis(2-chloroacetamido)diphenylsulfone (**Dac**)

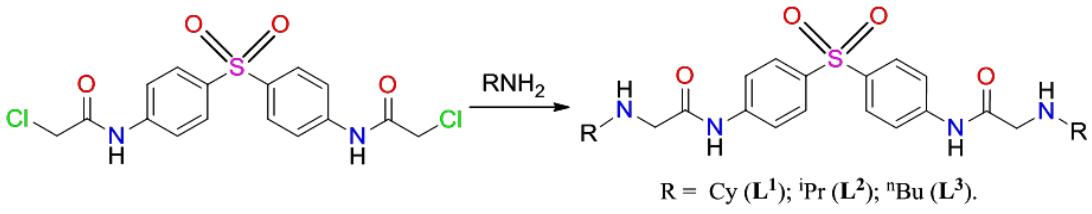

Scheme 2. Synthetic methodology for diamine precursors **L^{1}-L^{3}**

A room temperature single-pot reaction procedure involving self-assembly of the corresponding diamine **L^1-L^3** with CS_2 and transition metal ion viz. Ni^{II}, Cu^{II} or Zn^{II} affords access to a new series of bimetallic dithiocarbamate macrocyclic compounds **1a-1c, 2a-2c, 3a-3c** in moderate to good yields. The synthetic procedure is illustrated in Scheme 3. The affluence of synthesis and their prospective to be significant cytotoxic chemical species would further supplement the worth of the current series of bimetallic macrocyclic complexes.

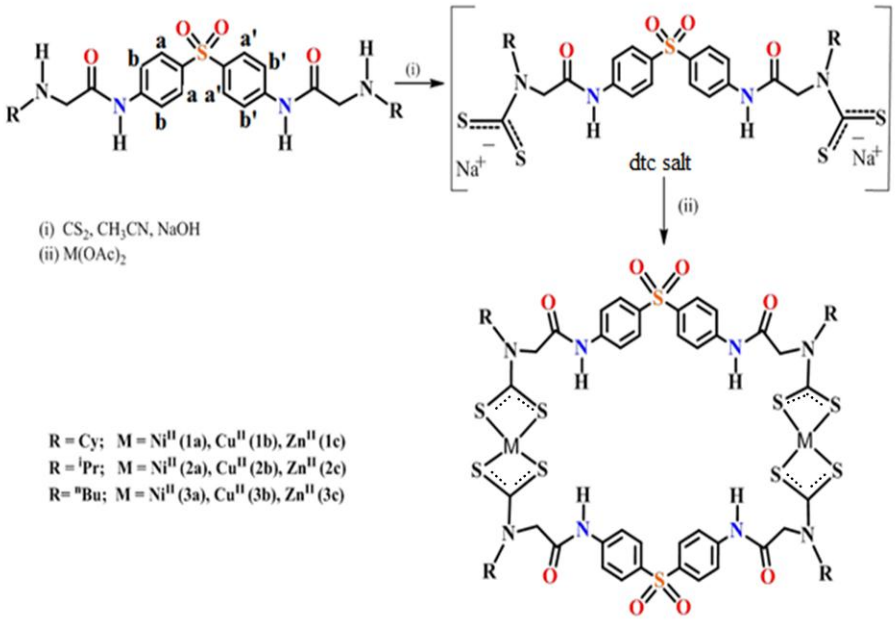

Scheme 3. One-pot synthetic protocol for binuclear metallomacrocyclic compounds 1a-1c, 2a-2c and 3a-3c.

While the newly synthesized compounds, **L^1-L^3** and bimetallic complexes **1a-1c, 2a-2c, 3a-3c** could not be obtained in the crystalline state, their composition and structures were confirmed by standard spectroscopic, thermogravimetric data and further verified by DFT study.

2.3.2. NMR, Mass and IR spectral study

Characteristic amine –NH signal could be seen in the ^{1}H NMR spectra of diamines as a broad peak in the range of 1.73-1.39 ppm. In the ^{1}H NMR spectra for **L^1-L^3**, the methylene group of N*CH*$_2$CO- linker and methine groups of N*CH*- substituents

are appeared in the range of 3.28-3.35 ppm and 2.31-2.70 ppm respectively. (Annexure 11 to Annexure 18**)**. It may be noted that a better splitting pattern is observed in the ^{1}H NMR spectrum of L^{2} recorded in $CDCl_3$, compared to similar spectrum recorded in DMSO-*d6*. ^{1}H NMR signals corresponding to the protons of aromatic and *N*-alkyl substituents appeared in the anticipated range as multiplets due to coupling with adjacent protons. The ^{13}C NMR spectra for **L^{1}-L^{3}** gave most characteristic signals in the range of 172-170 ppm, 56-50 ppm and 50.7-49.9 ppm are attributed to the carbonyl carbons, the α-methylene carbons (N*C*H_2CO) and aliphatic *N*-substituents (N*C*H/ N*C*H_2) respectively. The mass spectra of **L^{1}-L^{3}** gave molecular ion peaks corresponding to [M+H] along with expected fragments as shown in Annexure 1 to Annexure 3 respectively. In the IR spectra of **L^{1}-L^{3}**, a broad or multiple nature of ν (NH) vibration bands appeared which suggests the possibility of involvement of amide/amine functionalities in the intermolecular hydrogen bonding in the solid state. The appearance of a strong IR band in the region of 840-836 cm^{-1} due to the aromatic ν(C-H) out-of plane bending vibrations [16] confirms the presence of *para*-disubstituted benzene rings in these dap derivatives. (Annexure 7)

In the NMR spectra of the diamagnetic Ni^{II} (**1a, 2a** and **3a**) and Zn^{II} (**1c, 2c** and **3c**) complexes, signals corresponding to methine/methylene groups of N*CH*-/N*C*H_2-substituents and methylene group of N*C*H_2CO-linker, experience significant down-field displacements when compared to the respective diamino precursors. Notably, all the diamagnetic complexes displayed a very downfield signals in the range of 205.9 – 207.5 ppm in their ^{13}C NMR and confirms the presence of coordinated dithiocarbamate (-**N^{13}CS_2**) groups. Literature suggests that the metal-directed self-assembly of a discrete molecular structure depends on the stereo-electronic features of ligand framework,[17] metal centers [18] as well as thermodynamic conditions [19] The development of these metallomacrocyclic structures apparently profited from enthalpy as well as entropy effects over oligomeric or polymeric kinds. The appearance of expected signals and absence of signals from uncoordinated end groups in the NMR spectra ruled out the possibility of formation of oligomers or coordination polymeric entities. Annexure 19 to Annexure 24, Annexure 26 to Annexure 31**).** In support of this, we have recorded ^{1}H DOSY NMR spectrum of complex 2a **(**Annexure 25**)** 2c (Fig. 1) and 3c **(**Annexure 32**)** which unambiguously display the presence of only one type of species in solution.

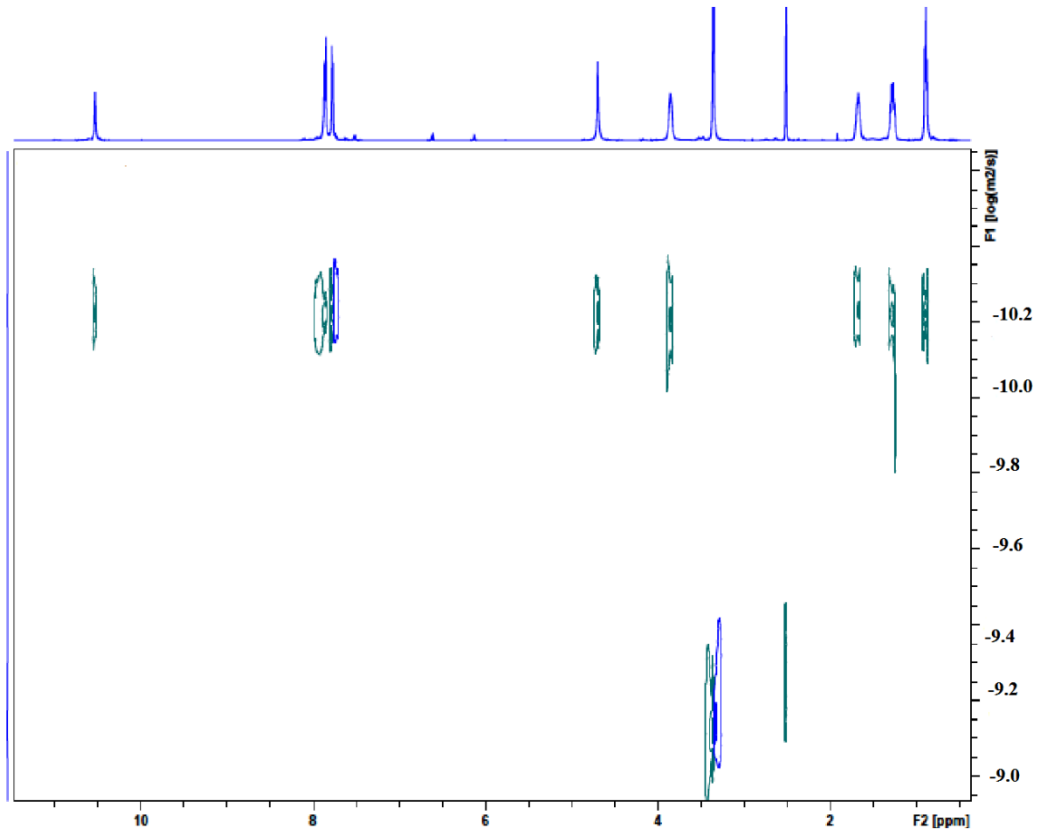

Fig. 1. DOSY NMR spectrum of 2c.

The mass spectra of $\mathbf{L^1}$-$\mathbf{L^3}$ and their metallomacrocyclic compounds gave molecular ion peaks which are either corresponding to [M+H], [M+Li], [M+Na] or [M+K] along with expected molecular fragments. The formation of the complexes 3a-3c is further confirmed by HRMS spectral data (Annexure 4 to Annexure 6). All the complexes displayed characteristic IR bands in the range of 1495–1403 cm^{-1} and ~1010 cm^{-1} due to ν(N-CSS) and ν_{as}(CSS) stretching vibrations, suggestive of an anisobidentate chelation of the dithiocarbamate ligand moieties in these complexes.[20] (Annexure 8 to Annexure 10). The NMR and IR spectral data are consistent with the analogous data reported by us [14, 20] recently.

2.3.3. UV-visible absorption, magnetic moment and florescence emission study

The ligand precursors $\mathbf{L^1}$-$\mathbf{L^3}$ exhibit a single prominent absorption band at shorter wavelength ~300 nm in their UV-visible absorption spectra and these bands are attributable to π→π* (phenyl) transitions. However, metallomacrocyclic compounds **1a-**

1c, 2a-2c, and **3a-3c** show two principal bands at ~ 300 nm and at ~ 450 nm attributable to π→π* (phenyl) and charge transfer transitions, respectively as shown in Fig. 2. Expectedly, copper complexes **1b, 2b** and **3b** display additional band at ~ 640 due to d-d transition. Overall, the UV-visible spectral data are consistent with the absorption behavior of metallomacrocyclic dithiocarbamate complexes of transition metals.[20] (Annexure 33). The magnetic moment values (Table 1) along with UV-visible absorption bands suggest a distorted square planar environment around Ni(II)/ Cu(II) and distorted tetrahedral environment around Zn(II) in their respective mononuclear dithiocarbamate complexes, which is further supported by DFT study, discussed in latter stage. Among the ligand precursors, $\mathbf{L^1}$ fluoresces maximum at 450 nm from locally excited π→π* transition states, however the rest of the ligand precursors displayed weak emission intensities. Interestingly, fluorescence property of diamine precursors $\mathbf{L^1}$-$\mathbf{L^3}$ has been quenched upon the formation of respective binuclear metallomacrocyclic complexes with nickel, copper and zinc. **(**Annexure 34**).** Although, nickel and copper ions are well known fluorescence quenchers, [20, 21] however, the fluorescence quenching behavior of zinc ions is found to be in contrast to the earlier observations[22] where zinc ions are involved to simulate the fluorescence properties of transition metal dithiocarbamate complexes. Literature suggests that the fluorescence property of the compounds is greatly affected by the molecular arrangements, non-covalent interactions and conformational rigidity of the fluorophores.

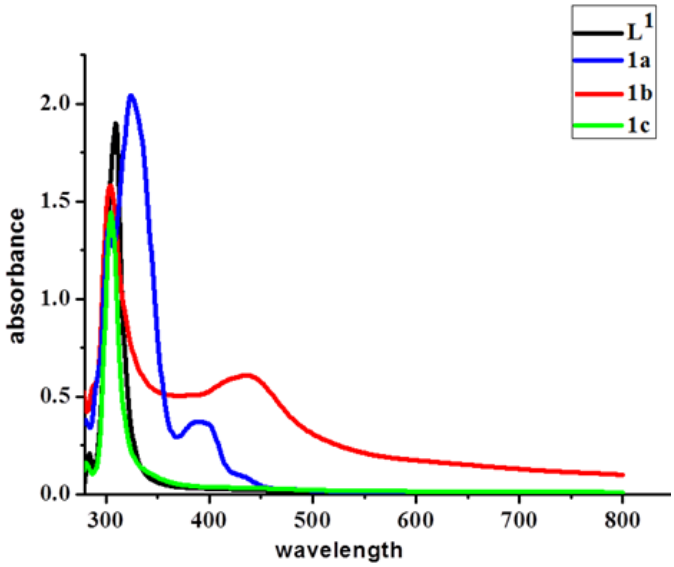

Fig. 2. UV–visible absorption spectra of compounds $\mathbf{L^1}$and **1a, 1b, 1c** in DMF solution.

Table 1

UV-visible absorption, magnetic moment and fluorescence data for the compounds

Entry	UV-visible spectral data (10^{-3} M DMF)	Magnetic Moment μ_{eff}(BM)	Fluorescence spectral data (10^{-3} M DMF)	
	λ_{max} nm (ε, L $Mol^{-1}cm^{-1}$)		λ_{ex} nm	λ_{em}(nm) (Intensity)
L^1	309(11385)π→π*	-	309	450 (475)
L^2	300 (2168) π→π*	-	300	445(19)
L^3	304 (6445)π→π*	-	304	449(29)
1a	324 (61261) π→π* 392 (11111) n→π* 432 (2402) charge transfer	dia	324	Non fluorescent
1b	304(15800) π→π* , 437(6000) charge transfer, 637(1500)*d-d transition*	1.83	304	500(14)
1c	305 (21621)π→π*, 434 (52612) charge transfer	dia	305	368 (63), 470 (65)
2a	299 (41500) π→π*, 324 (54962) π→π* 391 (8500) n→π*, 481 (1000)charge transfer	dia	299	Non Fluorescent
2b	301(25225) π→π*, 436 (6906) charge transfer, 640 (6006)*d-d transition*	1.88	301	Non fluorescent
2c	301 (35000) π→π*	dia	301	469(13)
3a	302 (37237) π→π*, 322 (47191) π→π* 389 (8108) n→π*, 482 (1201)charge transfer	dia	302	Non Fluorescent
3b	303 (18468) π→π*, 436 (8708) charge transfer 632 (6006) *d-d transition*	1.83	303	Non Fluorescent
3c	305 (19519) π→π*, 491 (1351) charge transfer	dia	305	Non Fluorescent

2.3.4. TGA/DTA study

The thermal decomposition patterns of metallomacrocyclic dithiocarbamate complexes **1a-1c, 2a-2c and 3a-3c** were studied by thermogravimetric method in the temperature ranges from room temperature to 550 ºC. **(**Annexure 35**).** Correctly, the heating rate was controlled at 10 ºC min^{-1} under nitrogen atmosphere. The temperature ranges corresponding to percentage weight loss during the decomposition, variable rate of decompositions observed on DTG curves and stable residual mass obtained for each complexes is summarized in Table S1. Thermogravimetric plots for these compounds (Fig. S49) clearly reveals a multistage mass loss on DTG curves and corresponding DTA peaks, attributed to endothermic and/or exothermic elimination of molecular fragments due to the thermal degradation. It may be noted that the thermal decompositions of all the

complexes start before their melting points and accompanied by the appearance of one or more endothermic peak on corresponding DTA curves. Further, it appears that complexes **1a** and **3c** are thermally unstable and their degradations start at a lower temperature (122-165ºC), compared to other complexes which are indeed stable up to ~216ºC. Except **1c**, all the complexes exhibit only ≈50% of degradations on TG curves and a stable residual mass could not be obtained up to 550 ºC. Complex **1c** displayed maximum degradation of 79.2 % of TG curve, giving a stable residual mass of 20.8 % which corresponds to ZnS (Calc. 13.12 %) plus char. Notably, thermal decomposition of zinc(II) complexes 1c and 3c is essentially taking place in a single stage giving a broad exothermic peak on DTA curve. The thermal data is consistent with the literature report where a thermal decomposition of similar dialkyldithiocarbamate transition metal (II) complexes [23] proceeds in several stages involving many exothermic processes.

2.3.5. Geometry Optimization

The DFT calculations have been widely used in recent years due to its ability to provide reasonably good results even for huge molecular structures. The DFT calculations have been successfully used by us [16, 20] recently to reproduce the geometries obtained by X-ray diffraction analysis. Thus, for a better understanding of the spectroscopic results, we accomplished full geometry optimizations of diamine precursor **L^1,** its dithiocarbamate salt **L^1**-dtc and its transition metal dithiocarbamate complexes **1a-1c** (Fig. 3) using density functional theory (DFT) at B3LYP/6-31G (d, p) and B3LYP/LanL2DZ basis sets, respectively. The structural parameters *viz* bond lengths and bond angles were found in good agreement with the X-ray data of closely related compounds.[24]

The DFT study clearly reveals that both the phenyl groups of **L^1** forms a dihedral angle of 28.57º whereas the similar angle in its transition metal dithiocarbamate complexes **1a-1c** appeared in the range of 77.74º -86.69º and confirms the existence of diversified *'gauche'* conformation. Further, it reveals the loss of coplanarity of amide groups and substantial deviations in the electronic structural parameters such as Ar-S-Ar angles in **1a-1c** (Table 2). For instance, Ar-S-Ar bond angle of 163.83º in **L^1** decreases significantly upon formation of its complexes **1a-1c**. Thus the flexibility associated with the –

$(CH_2CONHC_6H_5)_2SO_2$– linker framework of the ligand precursors would be an important factor; not only responsible for the formation of macrocyclic structure but also for their effective interactions with biomolecules. Moreover, optimized geometry of the dithiocarbamate salt of **L[1]** (Fig. 3) gave mutually trans disposition of dithiocarbamate moieties which apparently undergo a flip during their incorporation into the coordination with various transition metals in **1a-1c**. Substantial flipping of ligand moieties has been observed by us[25] previously during cluster growth reactions.

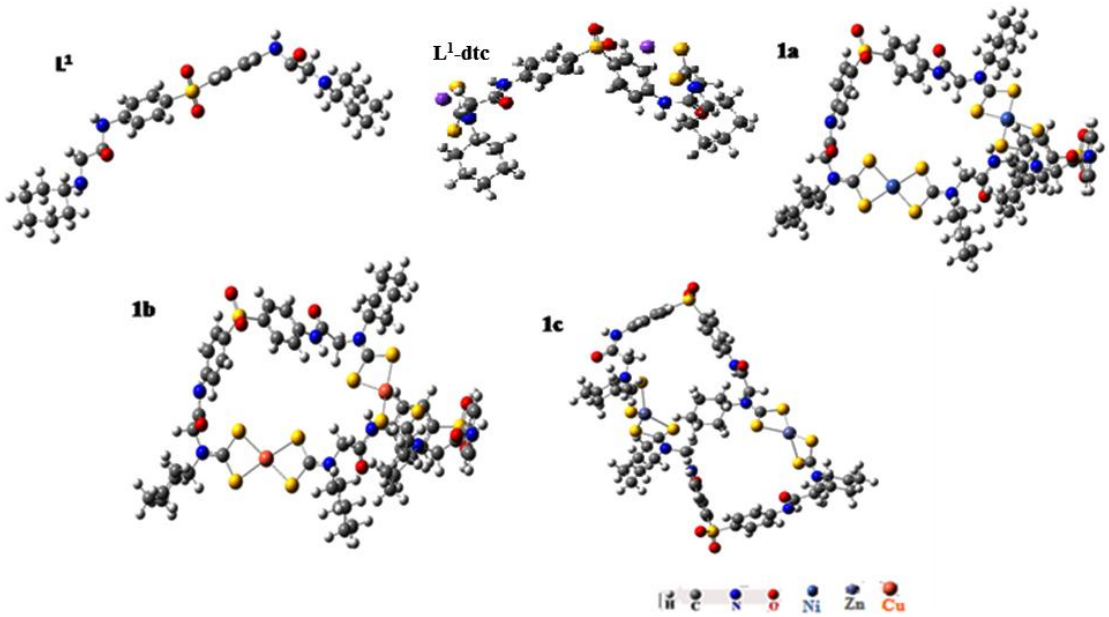

Fig. 3. An optimized geometry for the minimum energy conformation for **L[1]**, its dithiocarbamate salt **L[1]-dtc** and complexes **1a-1c**.

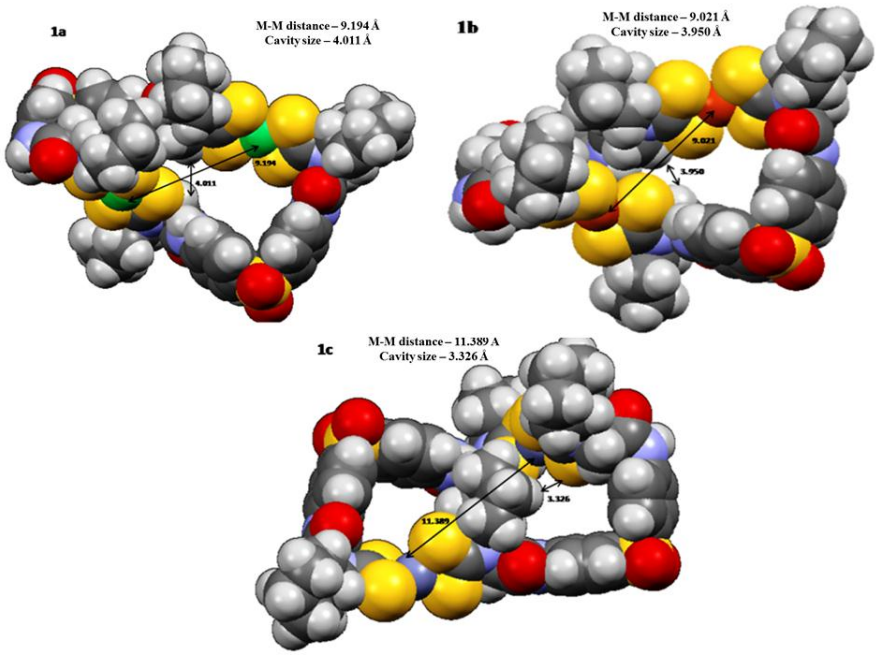

Fig. 4. Spacefilled representation of the optimized geometry revealing a cavity generated by the macrocyclic architecture of metallomacrocyclic dithiocarbamate complexes.

Selected bond lengths and bond angles of complexes **1a-1c** (Table 2) are found inconsistent with the similar parameters of the analogous structure [24a-24c] deduced experimentally by means of single crystal XRD and require no further comment here.

Table 2
Comparison of selected geometrical parameters for **1a-1c** obtained from theoretical with similar experimental parameters retrieved from the literature.

Selected Bond	Bond lengths (Å)	Selected Bonds	Bond angles (º)
	1a		
N—C	1.33-1.34	S—Ni—S (chelate)	77.87-78.24
C—S	1.72-1.75	S—Ni—S	100.13-103.95
Ni—S	2.27-2.28	C-S-C	100.33, 100.12
TransannularNi-Ni	9.194		
	Ni(II) dithiocarbamate based macrocycle [24a]		
N—C	1.281-1.508	S—Ni—S (chelate)	78.99-79.87
C—S	1.691-1.744	S—Ni—S	100.31-177.14
Ni—S	2.164-2.225	-	-
	1b		
N—C	1.34	S—Cu—S (chelate)	73.94-75.21
C—S	1.73-1.74	S—Cu—S	102.56-114.47
Cu—S	2.39-2.41	C-S-C	100.60, 101.09
TransannularCu-Cu	9.021		

Cu(II) dithiocarbamate based macrocycle[24b]			
N—C	1.318-1.328	S—Cu—S (chelate)	77.59
C—S	1.719-1.727	S—Cu—S	101.72-103.48
Cu—S	2.288-2.301	-	-
1c			
N—C	1.34	S—Zn—S (chelate)	75.08-75.91
C—S	1.74-1.76	S—Zn—S	126.03-129.37
Zn—S	2.42-2.47	C-S-C	103.98, 102.66
Transannular Zn-Zn	11.389		
Zn(II) dithiocarbamate based macrocycle[24c]			
N—C	1.333-1.363	S—Zn—S (chelate)	79.5-81.2
C—S	1.717-1.782	S—Zn—S	126.53-136.00
Zn—S	2.32-2.44	-	-

The geometries of **1a-1c** clearly suggest that two ligand molecules bridges over two metal centres *via* chelating sites of terminal dithiocarbamates resulted into the formation of binuclear dithiocarbamate macrocyclic compounds having distorted square planar geometry around nickel(II)/ copper (II) centers and distorted tetrahedral geometry around zinc(II) center in 1a-1c complexes respectively. One of the four *N*-Cy substituents in the macrocyclic architecture of **1c** is projected towards the inner side of the 44-member molecular cavity which can be visualized in the optimized geometry (Fig. 3) and in the spacefilled model (Fig. 4) of **1c**. An isobidentate coordination mode of the -NCS_2 moieties is clearly reflected by the appearance of almost similar M-S bond distances of 2.27-2.28 Å and 2.39-2.41 Å in nickel(II) **1a** and copper(II) **1b** complexes whereas in zinc(II) complex **1c**, these show anisobidentate coordination modes with appreciably different M-S bond distances of 2.32-2.44 Å. These observations are in accord with the experimental data and with the theoretical data calculated by us recently[20] on similar type of complexes. The transannular M···M distances of 9.194, 9.021 and 11.389 calculated from these 44-membered macrocycles **1a-1c**, respectively, are significantly smaller than the similar distances obtained experimentally for 33 membered macrocycles,[26] however, these are comparable to those of analogous systems.[20] The macrocyclic cavity seems to be hydrophobic because sulfur atoms are inclined inwards.

2.3.6. Electrochemical study

The biological relevance of dap and its derivatives has been emphasized in the introduction section of this contribution and it has appeared that the methods available for analysis of the drug in pharmaceutical dosage forms and biological fluids include spectrophotometry[27-29] electrochemical[30-32] and HPLC[33] etc to establish the stability of drug under different stress conditions, acid, basic, and oxidative. Thus, it was pertinent to investigate the electrochemical behavior of newly synthesized compounds as a large part of the biological activity of chemical species are related to their electron-transfer ability.[30-32] The electron-transfer ability of the ligand precursors $\mathbf{L^1}$-$\mathbf{L^3}$ and their dithiocarbamate complexes in 1.0 mM DMF solutions were investigated in the potential ranges +1.5 to -1.5 V. The experiments were performed with a one-compartment cell having a platinum-disk working electrode, a platinum-wire counter electrode and an Ag/Ag+ (in DMF) reference electrode. Voltammograms were recorded by using anhydrous solutions of $\mathbf{L^1}$-$\mathbf{L^3}$ and the metal complexes in dimethylformamide containing n-Bu_4NPF_6 (5 mM) as supporting electrolyte at a scan rate of 0.05 Vs^{-1}. All solutions were purged with N_2 for 30 min prior to each set of experiments.

Similar to the electrochemical response of dap,[30] the ligand precursors as well as their complexes displayed one well irreversible oxidation peak between -1.410V to -1.126 V during anodic scan at a sweep rate of 0.05 V/s (Fig. 5). Reportedly, the electrochemical behavior of dap was found to be affected by the solution pH and the type of supporting electrolyte where a substantial decrease in anodic peak current was seen as the pH of the solution has increased. The voltammograms of all the complexes (except copper complexes **1b, 2b** and **3b**) examined in this work, did not display any additional peak, compared to the cyclic voltammograms of $\mathbf{L^1}$-$\mathbf{L^3}$, in the cathode or anodic scan under the similar experimental conditions. This clearly demonstrates that these complexes are primarily electro active with respect to the coordinated ligands and the metal centers are present in silent mode. Contrarily, the cyclic voltammogram of copper complexes displays additional peak in the cathodic/anodic scans at less negative potentials (Fig. 5), apparently corresponds to the Cu^{II}/Cu^{I} redox couples. The separation between the anodic and cathodic peaks, $\Delta Ep = Epa - Epc$, is 0.55 V which is larger than $\Delta Ep = 0.059/n$ V and the ratio of the current intensity of the cathodic and anodic peaks is different from the

unity which suggests a quasi-reversible process [21] essentially taking place at copper center in these complexes. Subsequently the irreversible oxidation peak (vide supra) is shifted towards negative potential significantly due to the increase in the electron density after initial electroreduction of Cu(II) centers in the respective complex.

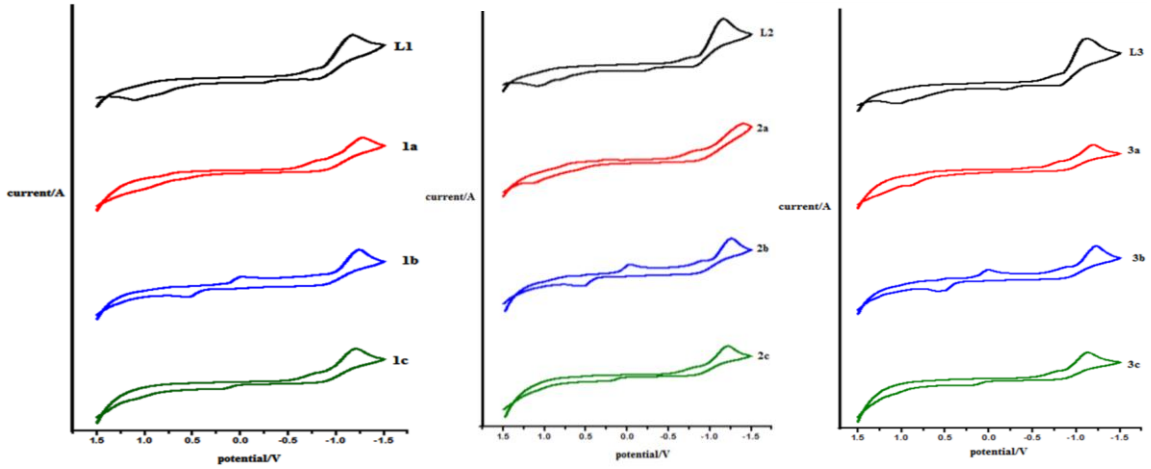

Fig. 5. CV curves of DMF solutions (5 mM n-Bu_4NPF_6) of the complexes **1a-1c, 2a-2c, 3a-3c** and **L^1, L^2, L^3** Scan rate: 0.05 V s^{-1}.

2.3.7. In vitro cytotoxic activity

The lead compound dap and its all derivatives Dac, **L^1-L^3**, **1a-1c**, **2a-2c** and **3a-3c** were screened for their possible *in vitro* cytotoxic activity by MTT assay against the malignant tumor cell lines Hep G2 (Hepatoma) and C6 (Glioblastoma). Further, **L^1** and its transition metal dithiocarbamate complexes **1a-1c** were tested against normal (non-carcinoma) cell lines under the similar condition. The cytotoxicity observed for these compounds were compared with the clinically used antineoplastic drug cisplatin [**C**]. The 50% inhibition concentration (IC50) values obtained after incubation for 24hrs for all the compounds against both the cell lines are summarized in Table 3 and Fig. 6.

Table 3 IC_{50} values for the entries **1-15** against Hep G2 and C6 cancer cells.

Entry	Compounds	Cytotoxicity IC50 (µg/ml) ± SE		
		Hep G2	C6	WRL-68
1	4,4'-bis(2-(cyclohexylamino)acetamido)diphenylsulfone (L^1)	32.35±0.011	17.78±0.018	163.80
2	4,4'-bis(2-(isopropylamino)acetamido)diphenylsulfone (L^2)	6.12±0.012	48.7±0.007	-
3	4,4'-bis(2-(n-butylamino)acetamido)diphenylsulfone (L^3)	56.1±0.032	32.2±0.010	-
4	$[Ni_2$-μ^2-bis-{(κ^2S,S-$S_2CN(Cy)CH_2CONHC_6H_4)_2SO_2$}] (1a)	16.21±0.017	54.95±0.019	>1000
5	$[Cu_2$-μ^2-bis-{(κ^2S,S-$S_2CN(Cy)CH_2CONHC_6H_4)_2SO_2$}] (1b)	19.95±0.016	15.13±0.018	381.30
6	$[Zn_2$-μ^2-bis-{(κ^2S,S-$S_2CN(Cy)CH_2CONHC_6H_4)_2SO_2$}] (1c)	21.37±0.023	32.35±0.017	383.14
7	$[Ni_2$-μ^2-bis-{(κ^2S,S-$S_2CN(^iPr)CH_2CONHC_6H_4)_2SO_2$}] (2a)	25.0±0.015	84.7±0.042	-
8	$[Cu_2$-μ^2-bis-{(κ^2S,S-$S_2CN(^iPr)CH_2CONHC_6H_4)_2SO_2$}] (2b)	66.4±0.037	137.0±0.015	-
9	$[Zn_2$-μ^2-bis-{(κ^2S,S-$S_2CN(^iPr)CH_2CONHC_6H_4)_2SO_2$}] (2c)	8.47±0.016	4.3±0.019	-
10	$[Ni_2$-μ^2-bis-{(κ^2S,S-$S_2CN(^nBu)CH_2CONHC_6H_4)_2SO_2$}] (3a)	27.7±0.020	59.33±0.015	-
11	$[Cu_2$-μ^2-bis-{(κ^2S,S-$S_2CN(^nBu)CH_2CONHC_6H_4)_2SO_2$}] (3b)	64.18±0.020	77.6±0.015	-
12	$[Zn_2$-μ^2-bis-{(κ^2S,S-$S_2CN(^nBu)CH_2CONHC_6H_4)_2SO_2$}] (3c)	25.8±0.016	25.0±0.017	-
13	Dapsone (dap)	26.3±0.016	18.4±0.008	-
14	4,4'-bis(2-chloroacetamido)diphenylsulfone (Dac)	5.78±0.016	6.25±0.014	-
15	Cisplatin (C)	22.7±0.025	16.8±0.018[34]	>80[35]

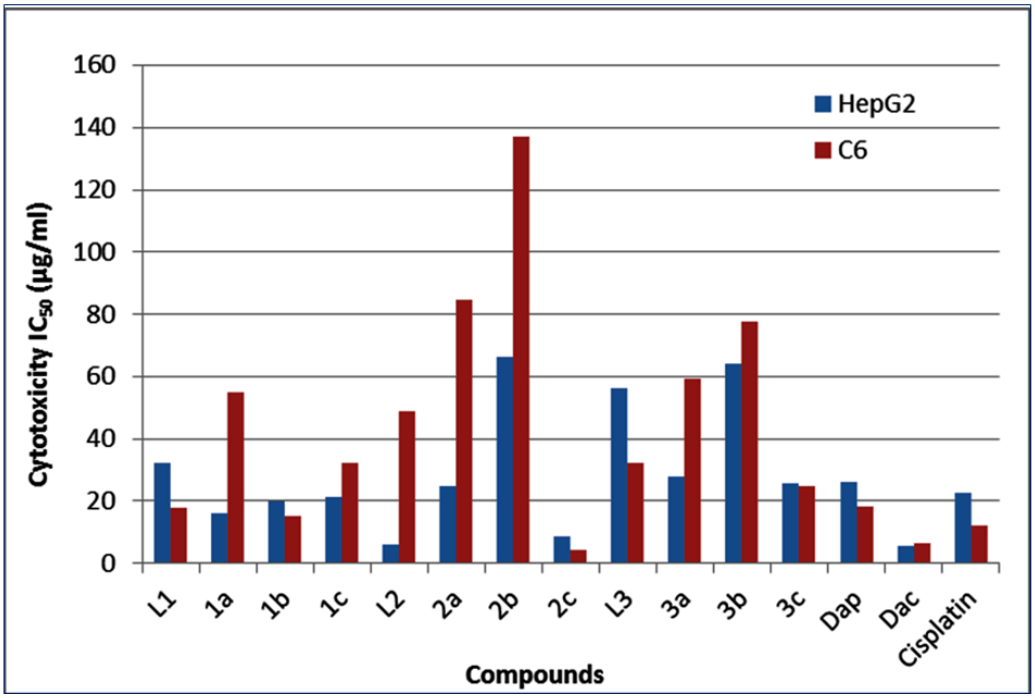

Fig. 6. Cytotoxicity IC_{50} (µg/ml) values for the lead compounds Dac and its all derivatives.

The overall result suggests that the synthesized compounds showed specificity for cancer cells over normal liver cells. Precisely, the first derivative of the lead compound

Dac exhibits pronounced cytotoxicity against both the cell lines (Fig. 6). Although Dac could not preserve the activity upon formation of its $\mathbf{L^1}$ and $\mathbf{L^3}$, derivatives, however the cytotoxicity of $\mathbf{L^1}$ and $\mathbf{L^3}$ is apparently augmented upon formation of its transition metal dithiocarbamate complexes against Hep G2 cell line. The IC50 value of the complexes **1a-1c** (Table 3) confirms their enhanced cytotoxicity than the reference drug Cisplatin (IC50= 22.7µg/mL). Amongst these, compound **1a** holding nickel (II) shows the optimum activity **(**IC 50 = 16.21 µg/ml**)**. The complexes **3a-3c** derived from $\mathbf{L^3}$ containing *N*-^{n}butyl substituent could not display better activity than cisplatin the against Hep G2 cell line. Interestingly, the activity of **Dac** is upheld upon the formation of $\mathbf{L^2}$ however its activity falls down significantly upon the formation of transition metal dithiocarbamate complexes **2a** and **2b** which is indeed contrary to the cytotoxicity trend observed with $\mathbf{L^1}$ and $\mathbf{L^3}$. Exceptionally, complex **2c** holding zinc(II) and *N*-^{i}Pr substituents shows nearly 3 fold better cytotoxic activity against both Hep G2 (8.47±0.016 µg/mL) and C6 (4.3±0.019 µg/mL) cell lines, compared to the reference drug Cisplatin. In general, low cytotoxicity profile for all newly synthesized compounds (Except **Dac, 1b** and **2c**) was observed against C6 (glioblastoma cell line) as compared to their activity against Hep G2 cells and reference drug cisplatin. This may apparently arises due to the fact that brain especially glial cells behave differently compared to other cells of the body.[14a] The discrepancy may be attributed to the reason that the brain is separated by a strong blood brain barrier which principally decides what molecules to pass and what to block.

Apoptosis or “programmed cell death” is a key process during cell development, maintaining cell populations in tissues, immune system and aging. Apoptosis also plays a crucial role in many pathological conditions like cancer for natural tumor suppression and cancer treatment which eliminate abnormal malignant cells and reduce tumor size. DNA fragments resulting from apoptosis are visualized after separation by gel electrophoresis. Caspase-activated DNase (CAD) is involved as a key event in apoptosis wherein the DNA degraded at internucleosomal linker regions, resulting in DNA fragments that are multiples of 180–185 base-pairs in length. Separation of these fragments by agarose gel electrophoresis and subsequent visualization by ethidium bromide staining, results in a characteristic "ladder" pattern. DNA laddering can be used as a final state read-out

method and has therefore become a reliable method to identify apoptosis.[36a] Thus morphological investigations were carried out by using microscopic photographs of both the cell lines Hep G2 and C6 upon 24 h exposure to the lead compound dap along with all the newly synthesized compounds **Dac, L^1**, **L^2**, **L^3** and their ensuing transition metal dithiocarbamate complexes **1a-1c**, **2a-2c**, **3a-3c** as well as standard cisplatin at their respective *in vitro* IC_{50} values (Supporting Information). The microscopic photographs for most potent compounds are shown in Fig. 7, where A and D show normal proliferation of cells without any insult, B and E show the effect of zinc(II) dithiocarbamate complex **2c** on cell growth, whereas C and F show fewer proliferation of cells due to the exposure of compound **Dac**. The shrinking of cells, a characteristic apoptotic sign,[36b] indicating the induction of apoptosis as part of the mechanism of action of these compounds can be clearly visualized from the photographs. The mode of action of these compounds was further reinforced by DNA ladder assay. Thus, DNA laddering was performed upon treatment of the representative compounds on hepatocellular carcinoma Hep G2 cell line. The present study confirms a moderate to heavy DNA laddering of Hep G2 cell line upon treatment with **L^1** and its dithiocarbamate complexes **1a-1c**. The intra- nucleosomal DNA fragmentation (laddering) in the form of a ladder due to endonucleolytic attack is clearly envisaged in Fig. 8.This is considered as one of the later steps in smearing of DNA due to necrosis. The morphological changes and DNA laddering clearly demonstrate the induction of apoptotic cell death, required for major chemical therapeutic implications.

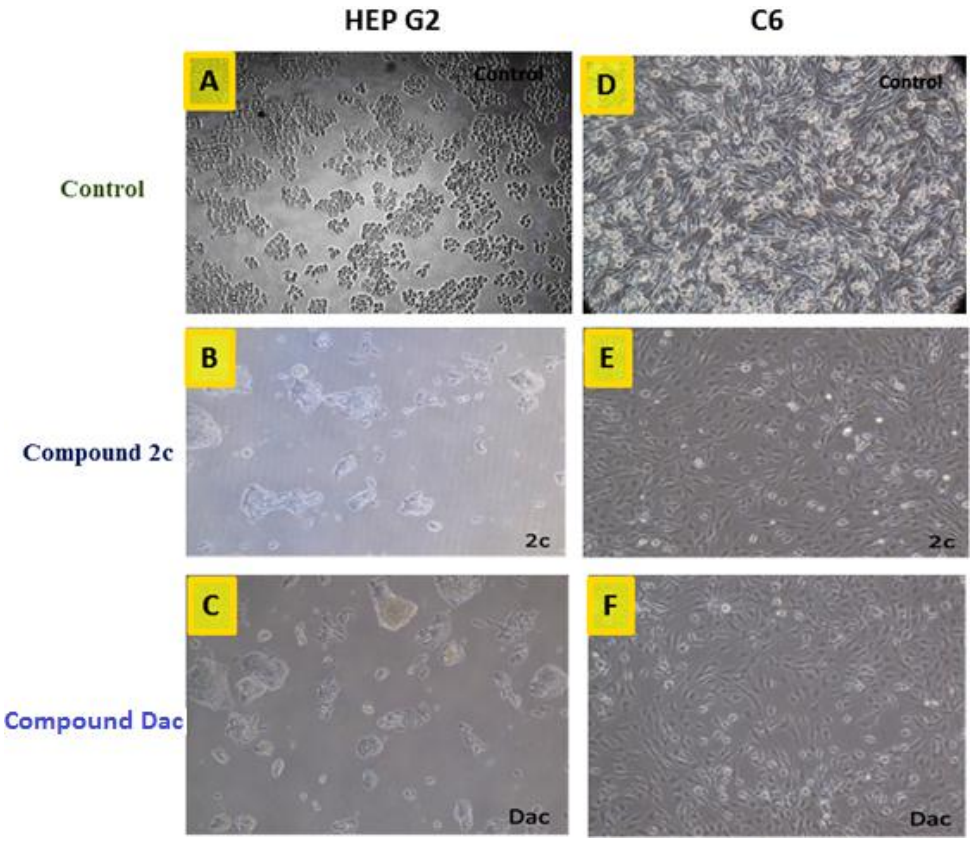

Fig.7. Phase Contrast Images of Hep G2 and C6 cells exposed to the potential compounds **2c** (middle row) and **Dac** (lower row) compared to control (top row) indicating the *in-vitro* cytotoxic activity. These compounds were assayed at their respective *in-vitro* growth inhibitory IC_{50} value, as determined using the MTT assay in Hep G2 and C6 cells.

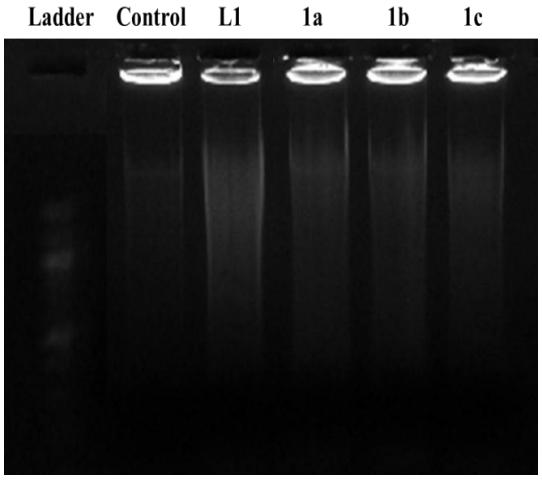

Fig. 8. DNA fragmentation assay in Hep G2 after treatment with L^1 and its complexes 1a, 1b and 1c (lane **1**: control (DMSO); lane **2**: L^1; lane **3**: 1a; lane **4**: 1b and lane **5**: 1c at the concentration of their respective IC_{50} values).

Thus, DNA could be the probable target for the cytotoxic activity[37a,37b] of these compounds as they can affect the primary structure of DNA along with prolonged and variable response in cells which may lead to cell death via regulated apoptosis.[38] In case of glioblastoma, studies have proven the noteworthy effect of dap as anti-VEGF and anti-angiogenic agent which deprives of neutrophil-mediated growth stimulating effects.[39] As observed in Hep G2 results, IC 50 values of **L^1**, **2a** and **3a** (IC 50= 32.35, 25.0, 27.7 is close to that of dap (IC 50= 26.3). Prior studies have also reported the role of dap in inhibiting G protein activation;[40] the molecular mechanism is however not well understood. Loss of G protein function has been very well studied to cause oncogenic behavior, thus providing a potential link for dap in the observed cytotoxicity results.

2.4. Conclusion

In continuation to our on-going research interest [14] on the evaluation of cytotoxic properties of relatively unexplored metallomacrocyclic dithiocarbamate complexes and in the light of a wide range of pharmacological activities exhibited by sulfone derivatives,[41-46] we have derivatize dap to obtained a novel series of organic diamines **L^1-L^3** and their ensuing transition metal metallomacrocyclic dithiocarbamate complexes **1a-1c**, **2a-2c**, **3a-3c**. All the new compounds were structurally characterized by FT IR, MS, ^{1}H, ^{13}C, ^{1}H DOSY NMR spectroscopy, UV-visible, fluorescence spectrophotometers and by thermogravimetric analysis. The geometry of the compounds has been optimized by density functional theory and electrochemical responses have also been investigated. All the newly synthesized compounds were screened for their *In vitro* cytotoxic activity against malignant human tumor Hep G2 (hepatoma) and C6 (Glioblastoma) cell lines by the MTT assay. Evidently, the first derivative of the lead compound **Dac** in its metal-free form and metallomacrocyclic complexes **1b** and **2c** exhibit higher cytotoxicity against both the cancer cells whereas **L^2** and **1a** exhibit higher cytotoxicity against Hep G2 specifically. Outstandingly, 4,4'-bis(2-chloroacetamido)diphenylsulfone (**Dac**) and metallomacrocyclic complex **2c** showed nearly 3 fold better cytotoxic activity against both Hep G2 (8.47±0.016 µg/ml) and C6 (4.3±0.019 µg/ml) cell lines, compared to the reference drug Cisplatin, and thereby these derivatives project themselves as a

better candidate for an cytotoxic drug. Moreover, DNA laddering and the morphological evidences suggest the induction of apoptotic cell death and explain the mode of action of these derivatives as cytotoxic agents. Relatively, deprived cytotoxicity of these compounds against C6 cell line, compared to their activity against Hep G2 cells may be attributed to the fact that the brain is separated by a strong blood brain barrier which principally decides what molecules to pass and what to block. The different reactivity of the same compounds against Hep G2 and C6 cell lines opens the scope for further investigations against other carcinoma human cell types.

2.5. References

[1] G. A. H. Buttle, D. Stephenson, S. Smith, T. Dewing, G. E. Foster, *Lancet* **1937**, *229*, 1331–1334.

[2] J. Adam, Esbenshade, H. Richard Ho, Ayumi Shintani, Zhiguo Zhao, Lesley-Ann Smith, L. Debra Friedman, *Cancer* **2011**, *117*, 3485-3492.

[3] a) Theonest Mutabingwa, Alexis Nzila, Edward Mberu, Eunice Nduati, Peter instanley, Elizabeth Hills, William Watkins, *Lancet* **2001**, *358*, 1218-1223; b) *T. Lang, B. Greenwood, Lancet Infect Dis.* **2003**, *3*, 162–168.

[4] L. Luzzatto, *The Lancet **2010**, 376*, 739–741.

[5] a) R. A. Ahmad, H. J. Rogers, Br. *J. Clin. Pharmacol*. **1980**, *10*, 519-524; b) J. Bernard Brabin, A. Teunis Eggelte, Monica Parise, Francine Verhoeff, *Drug Safety* **2004**, *27*, 633-648.

[6] F. A. Pieters, J. Zuidema, *Int. J Clin. Pharmacol. Ther. Toxicol*. **1987**, *25*, 396-400.

[7] a) J. Zuidema, E. S. Hilbers-Modderman, F. W. Merkus, *ClinPharmacokinet*. **1986**, *11*, 299-315; b) H. R. Winter, Y. Wang, J. D. Unadkat, *Drug Metab. Dispos*. **2000**, *8*, 865–868.

[8] D. G. May, J. A. Porter, J. P. Uetrecht, 0. R. Wilkinson, R. A. Branch, *Clin. Pharmacol. Ther*. **1990**, *48*, 619-627.

[9] R. Gelber, J. H. Peters, G. R. Gordon, A. J. Glazko, L. Levy, *Clin. Pharmacol. Ther*. **1971**, *12*, 225-238.

[10] a) E. M. Driggers, S. P. Hale, J. Lee, N. K. Terrett, *Nat. Rev. Drug Discov*. **2008**, *7*, 608-624; b) J. Mallinson, I. Collins, *Future Med Chem* **2012**, *4*, 1409-1438; c) A. Mann, Wermuth CG (Ed.) Academic Press, London, UK **2008**.

[11] a) C. N. R. Rao, S. Natarajan, R. Vaidhyanathan, *Angew. Chem., Int. Ed*. **2004**, *43*, 1466-1496; b) C. Ferey, C. Mellot-Draznieks, C. Serre, F. Millange, *Acc. Chem. Res*. **2005**, *38*, 217-225.

[12] J. L. C. Rowsell, O. M. Yaghi, *Angew. Chem., Int. Ed*. **2005**, *44*, 4670-4679.

[13] S. J. Lippard, *Pure Appl. Chem*. **1987**, *59*, 731-742.

[14] a) V. K. Singh, R. Kadu, H. Roy, *Eur. J. Med. Chem*. **2014**, *74*, 552-561; b) R. Kadu, H. Roy, V. K. Singh, *Appl. Organomet. Chem.* **2015**, *29*, 746-755; c) V. K. Singh, R. Kadu, H. Roy, P. Raghavaiah, S. M. Mobin, *Dalton Trans.* **2015**, *45*, 1443-1454; d) W. M. Pardridge, *NeuroRx*, **2005**, 2, 3-14.

[15] F. A Pieters, J. Zuidema, *Int. J. Clin. Pharmacol. Ther. Toxicol*. **1987**, *25*, 396-400.

[16] R. Kadu, V. K. Singh, S. K Verma, P. Raghavaiah, M. M. Shaikh, *J. Mol. Struct*. **2013**, *1033*, 298-311.

[17] G. Ercolani, *J. Phys. Chem. B*. **2003**, *107***,** 5052-5057.

[18] S. Leininger, B. Olenyuk, P. J. Stang, *Chem. Rev*. **2000**, *100*, 853-908.

[19] C. J. Jones, *Chem. Soc. Rev*. **1998**, *27*, 289-299.

[20] R. Kadu, V. Pillai, V. Amrit , V. K. Singh, *RSC Adv*. **2015**, ***5,*** 106688-106699.

[21] S. K. Verma, R. Kadu, V. K. Singh, *Nano-Met. Chem*. **2014**, *44*, 441-448.

[22] a) S. K. Verma, V. K. Singh, *RSC Adv*. **2015**, *5*, 53036-53046; b) S. K. Verma, V. K. Singh, *J. Organomet. Chem*. **2015**, *791*, 214-224.

[23] B. F. Ali, W. S. Al- Akramawi, K. H. Al- Obaidi, A. H. A. Al-Karboli, *Thermochimica Acta* **2004**, *419*, 39-43.

[24] a) P. D. Beer, A. G. Cheetham, M. G. B. Drew, O. Danny Fox, J. Elizabeth Hayes, T. D. Rolls, *Dalton Trans*. **2003**, *4*, 603–611; b) J. Cookson, E. A. L. Evans, J. P. Maher, C. J. Serpell, R. L. Paul, A. R. Cowley, M. G. B. Drew, P. D. Beer, *Inorg. Chim. Acta* **2010**, *363*, 1195–1203; c) Siu-Wai Lai, M. G. B. Drew, P. D. Beer, *J. Organomet. Chem*. **2001**, *637–639*, 89–93.

[25] P. Mathur, V. K. Singh, S. M. Mobin, C. Srinivasu, R. Trivedi, A. K. Bhunia, V. G. Puranik, *Organometallics* **2005**, *24*, 367-372.

[26] N. A. Celis, R. V.-Ramos, H. Höpfl, I. F. H.-Ahuactzi, M. Sánchez, L. S. Z.-Rivera, V. Barba, *Eur. J. Inorg. Chem*. **2013**, *16*, 2912-2922.

[27] H. D. Revanasiddappa, B. Manju, Drug Dev. *Ind. Pharm*. **2002**, *28*, 515-521.

[28] P. Nagaraja, K. R. Sunitha, R. A. Vasanth, H. S. Yathirajan, *Indian Drugs* **2001**, *38*, 489-490.

[29] H. D. Revanasiddappa, B. Manju, *J. Pharm. Biomed. Anal*. **2001**, *25*, 631-7.

[30] P. Manisankar, A. Sarpudeen, S. Viswanathan, *Biomed. Anal*. **2001**, *26*, 873-81.

[31] H. Oelschlaeger, G. Modrack, Arch. Pharm. **1986**, *319*, 10-14.

[32] H. Yang, X. Chen, W. Jiang, Y. Lu, *Inorg. Chem. Commun*. **2005**, *8*, 853–857.

[33] X.-L. Wang, H.-Y.Zaho, H.-Y.Lin, G.-C.Liu, J.-N.Fang, B.-K.Chen, *Electroanalysis* **2008**, *20*, 1055-1060.

[34] H. Yildirim, F. Kockar, C. Nakiboglu, *J. Nigerian Asso. Math. Phy.* **2012,** *11*, 12422-12428.

[35] A. A. Ibrahim, H. Khaledi, P. Hassandarvish, H. M. Ali, H. Karimian, *Dalton Trans*. **2014**, *43*, 3850-3860.

[36] a) S. Elmore, **2007**, 35, 495–516; b) M. P. Mattson, *Brain Pathol*. **2000**, *10*, 300-312.

[37] a) M. Boualam, R. Willem, M. Biesemans, M. Gielen, *Appl. Organomet. Chem*. **1991**, *5*, 497-506; b) M. Gielen, L. D. Clercq, R. Willem, E. Joosen, CRC Press, Boca Raton, FL, **1988**, 39–46.

[38] C. Pellerito, L. Nagy, L. Pellerito, A. Szorcsik, *J. Organomet. Chem*. **2006**, *691*, 1733-1747.

[39] R. E. Kast, A. Scheuerle, C. R. Wirtz, G. Karpel-Massler, *Chem*. **2011**, *11*, 756–761.

[40] S. M. Debol, M. J. Herron, , R. D. Nelson, *Bio*. **1997**, *62*, 827-836.

[41] J. N. Dominguez, C. Leon, J. Rodrigues, N. Gamboa De Dominguez, J. Gut, P. J. Rosenthal, *Eur. J. Med. Chem*. **2009**, *44*, 1457–1462.

[42] G. Szilágyi, T. Somorai, É. Bozó, J. Langó, G. Nagy, J. Reiter, J. Janáky, *Eur. J. Med. Chem*. **1990**, *25*, 95–101.

[43] C. Santelli-Rouvier, J.M. Barret, C.M. Farrell, D. Sharples, B.T. Hill, J. Barbe, *Eur J Med Chem*. **2004**, *39*, 1029–1038.

[44] J.M. Barret, C.M. Farrell, D. Sharples, B.T. Hill, J. Barbe, *Eur. J. Med. Chem*. **2004**, *39*, 1029–1038.

[45] T. Murafuji, Y. Fujiwara, D. Yoshimatsu, I. Miyakawa, K. Migita, Y. Mikata, *Eur. J. Med. Chem*. **2011**, *46*, 519–525.

[46] A. R. Usera, P. Dolan, T.W. Kensler, G.H. Posner, *Bioorg. Med. Chem*. **2009**, *17*, 5627–5631.

2.6. Annexures:

2.6.1. Spectral Characterization

Mass Spectra:

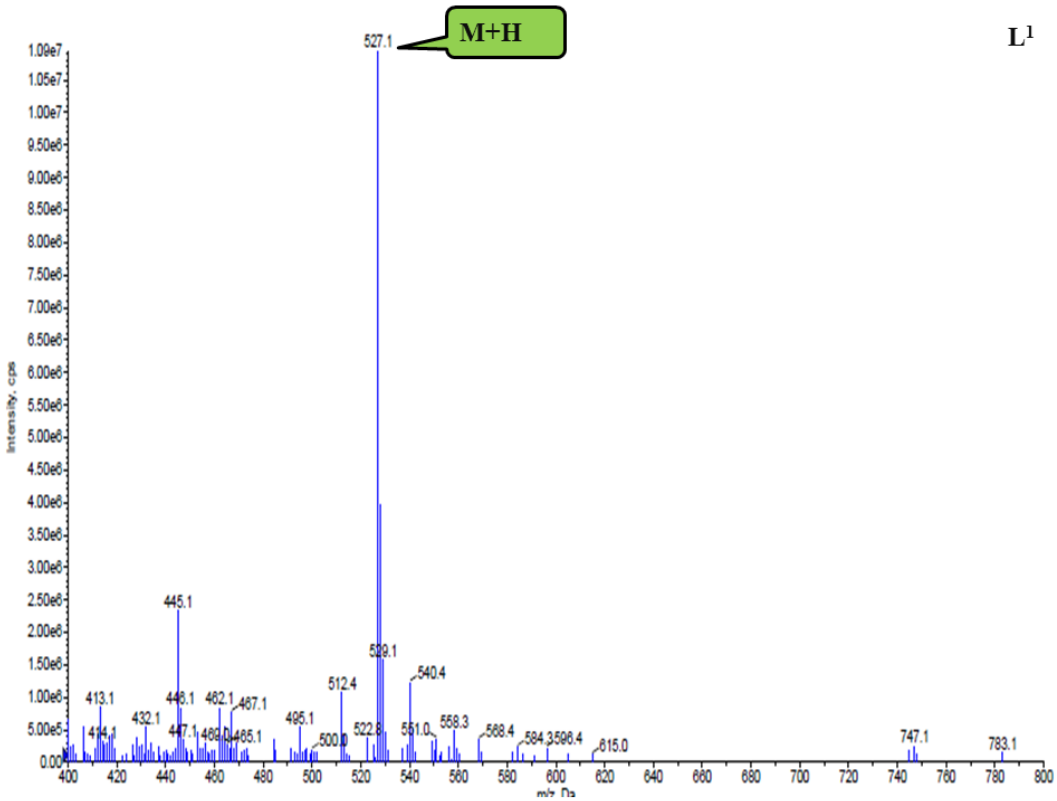

Annexure 1. ESI-MS spectrum of L^1.

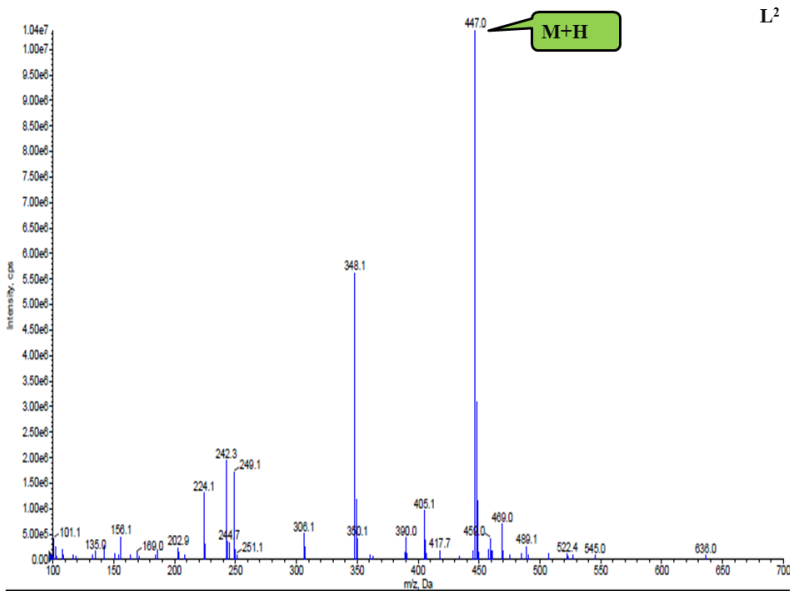

Annexure 2. ESI-MS spectrum of L^2.

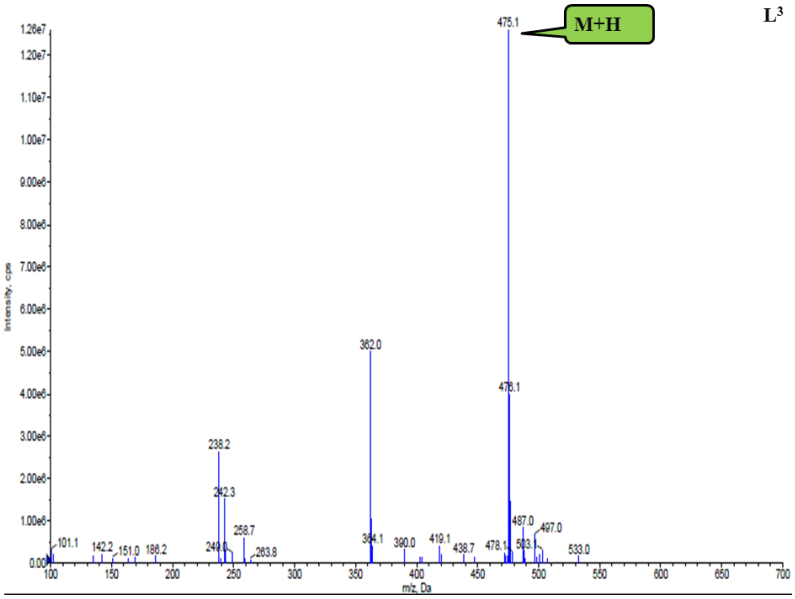

Annexure 3. ESI-MS spectrum of L^3.

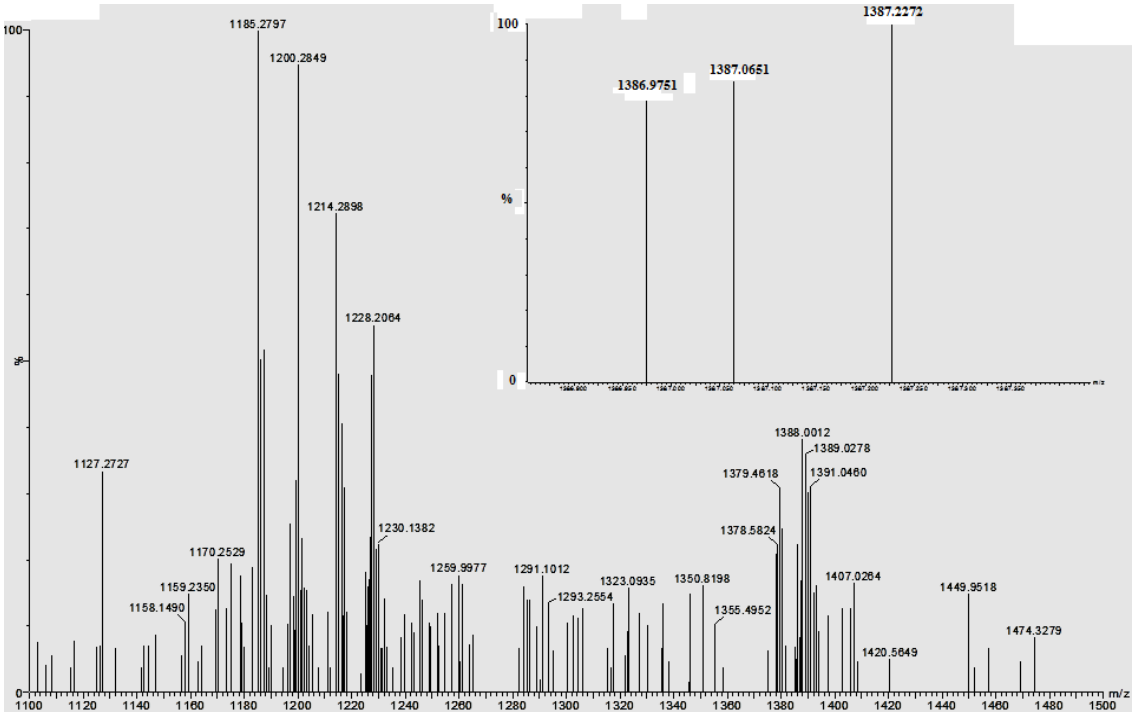

Annexure 4. HRMS spectrum of 3a; **inse**t: expanded spectrum.

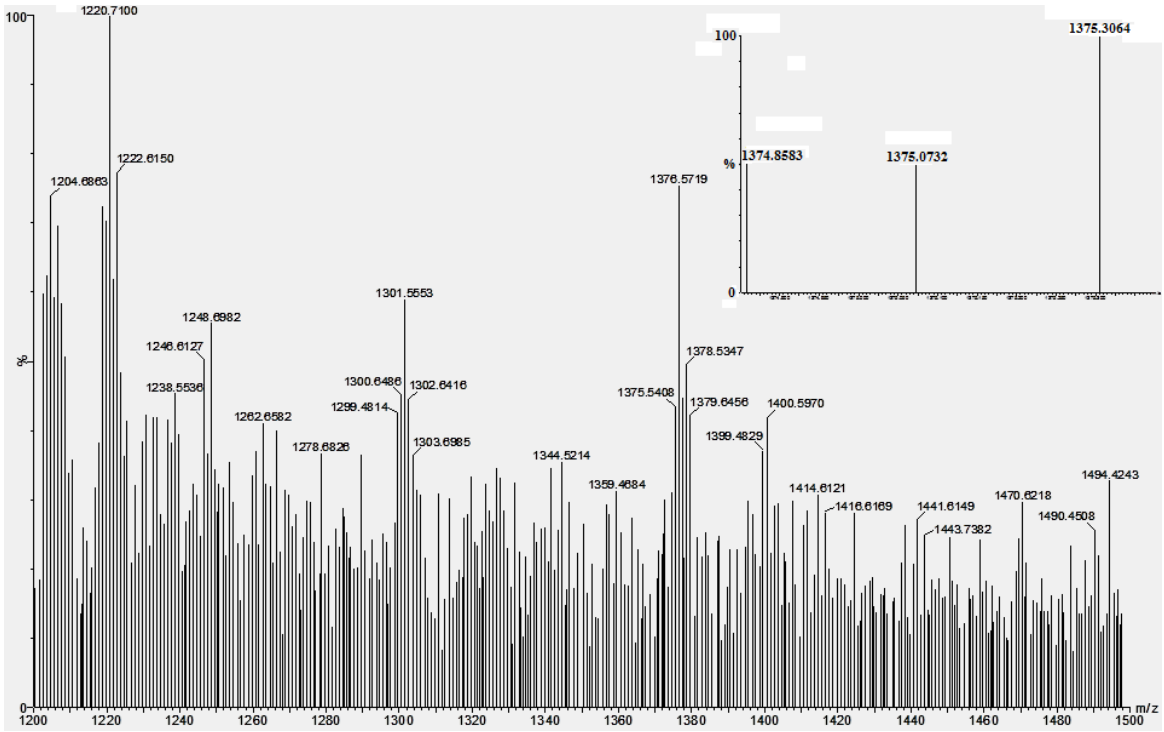

Annexure 5. HRMS spectrum of 3b; **inset:** expanded spectrum.

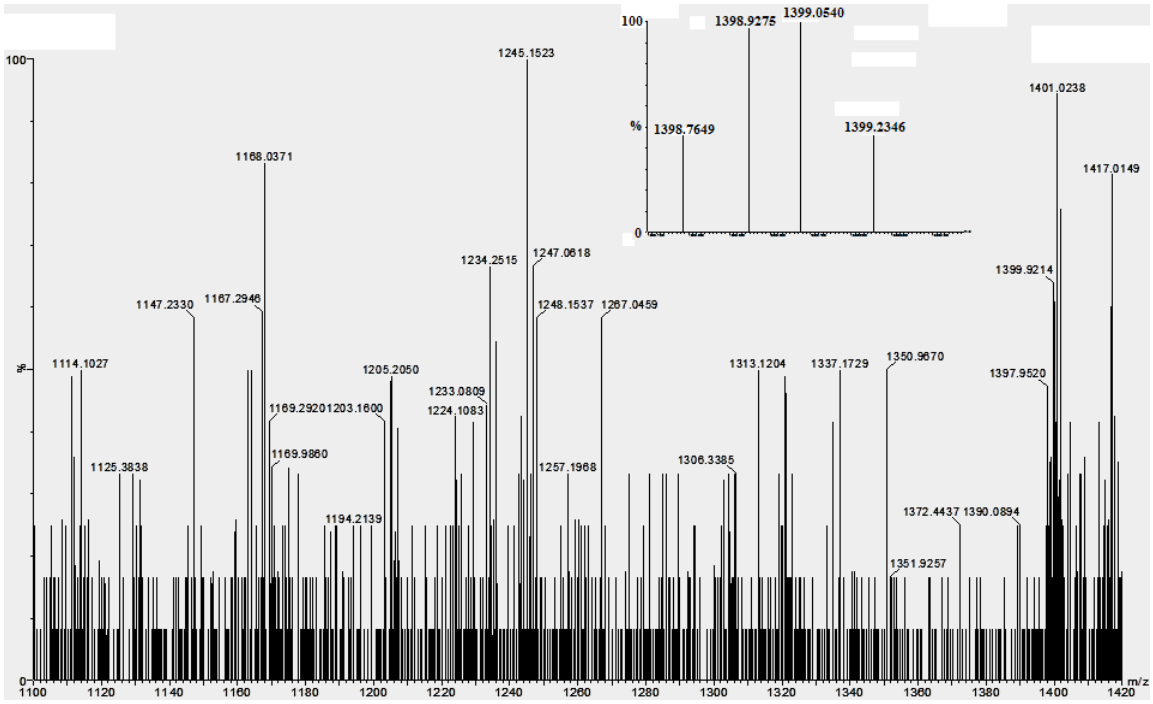

Annexure 6. HRMS spectrum of 3c; **inset**: expanded spectrum.

IR spectral data:

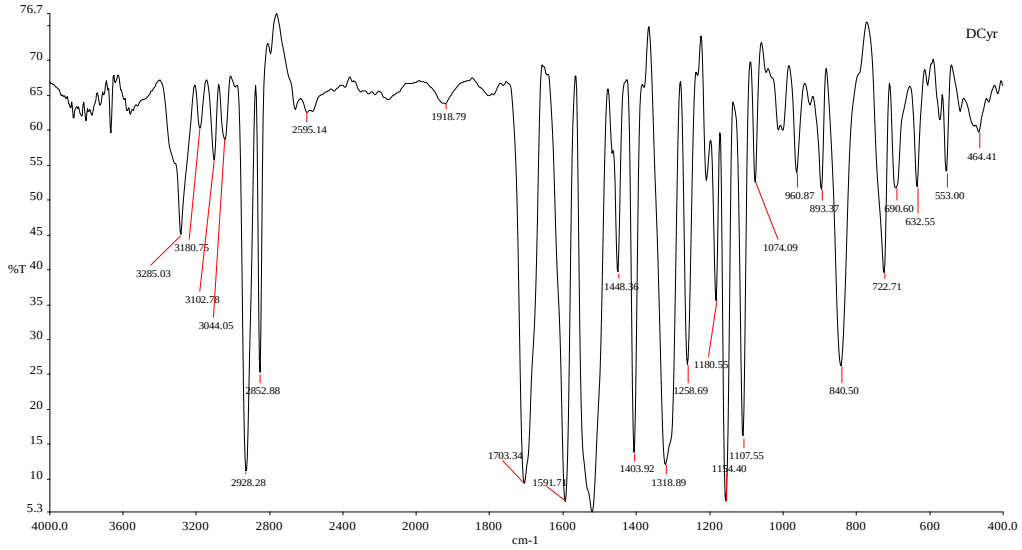

Annexure 7. IR spectrum of L^1

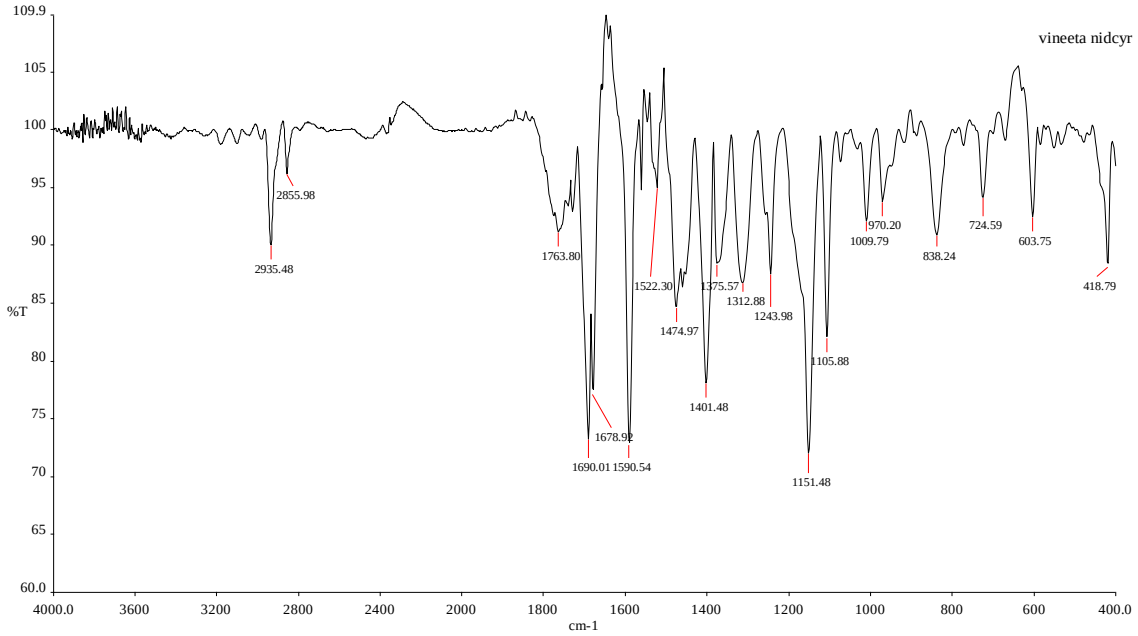

Annexure 8. IR spectrum of 1a

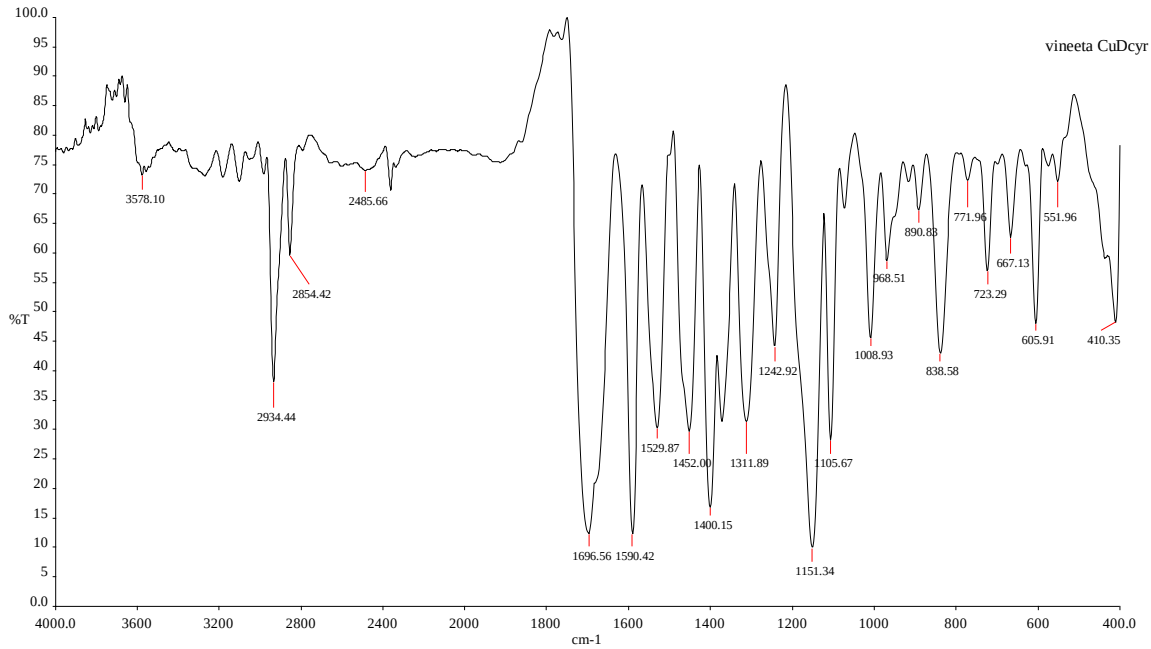

Annexure 9. IR spectrum of 1b

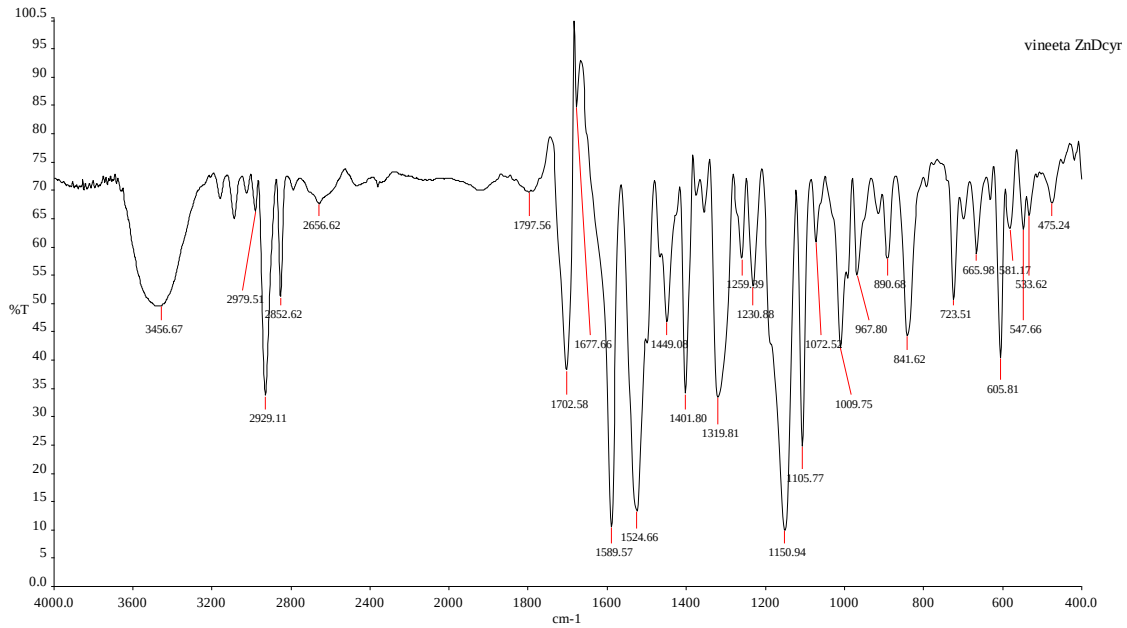

Annexure 10. IR spectrum of 1c

NMR spectral data:

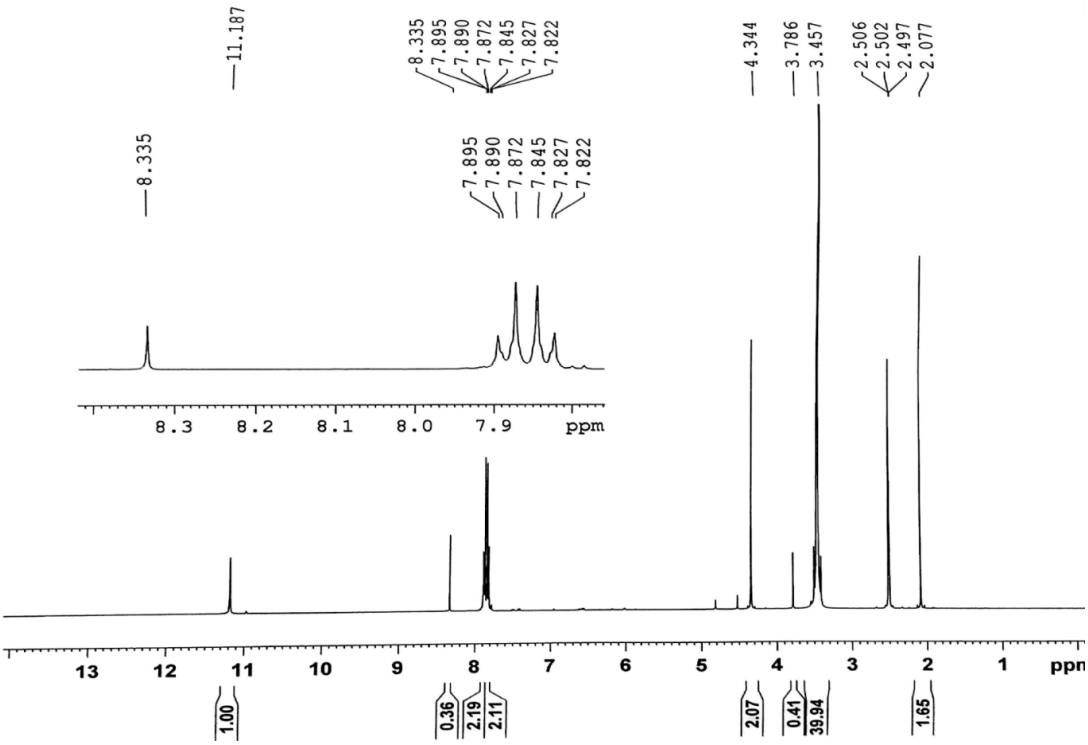

Annexure 11. ^{1}H NMR spectrum of Dac inDMSO-d_6.

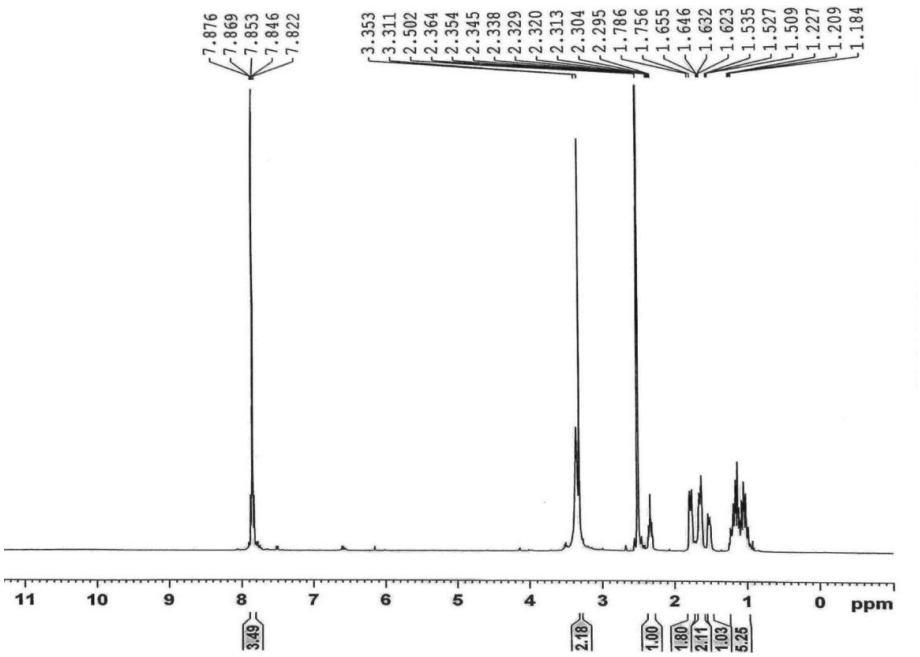

Annexure 12. ^{1}H NMR spectrum of L^1 in DMSO-d_6.

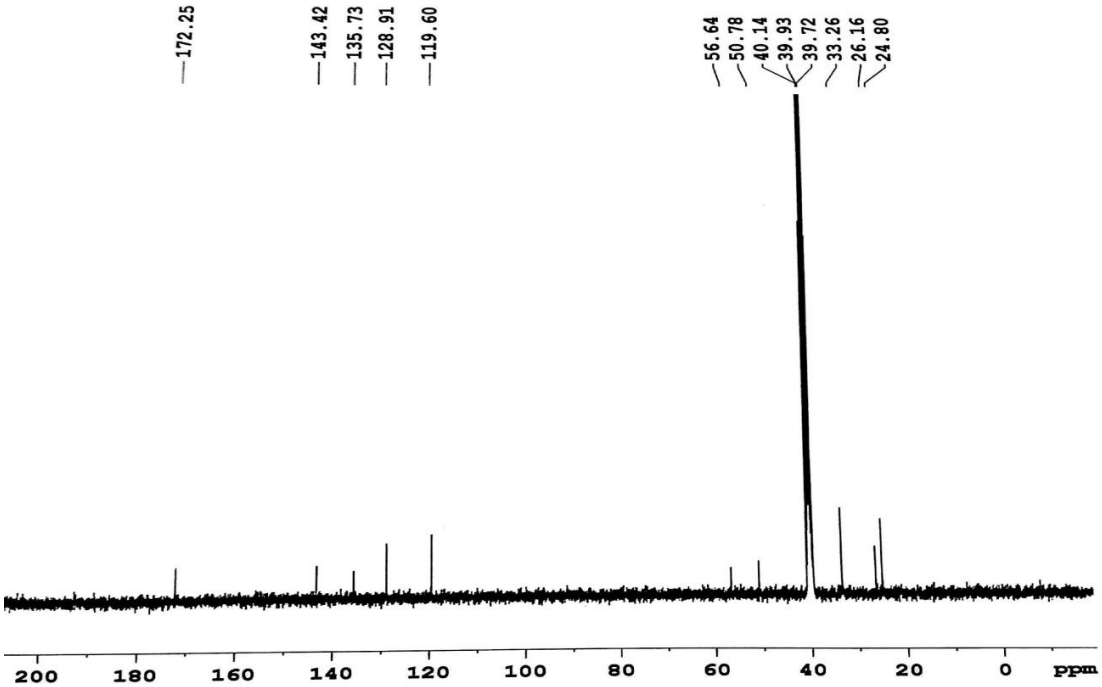

Annexure 13. ^{13}C NMR spectrum of L^1 in DMSO-d_6.

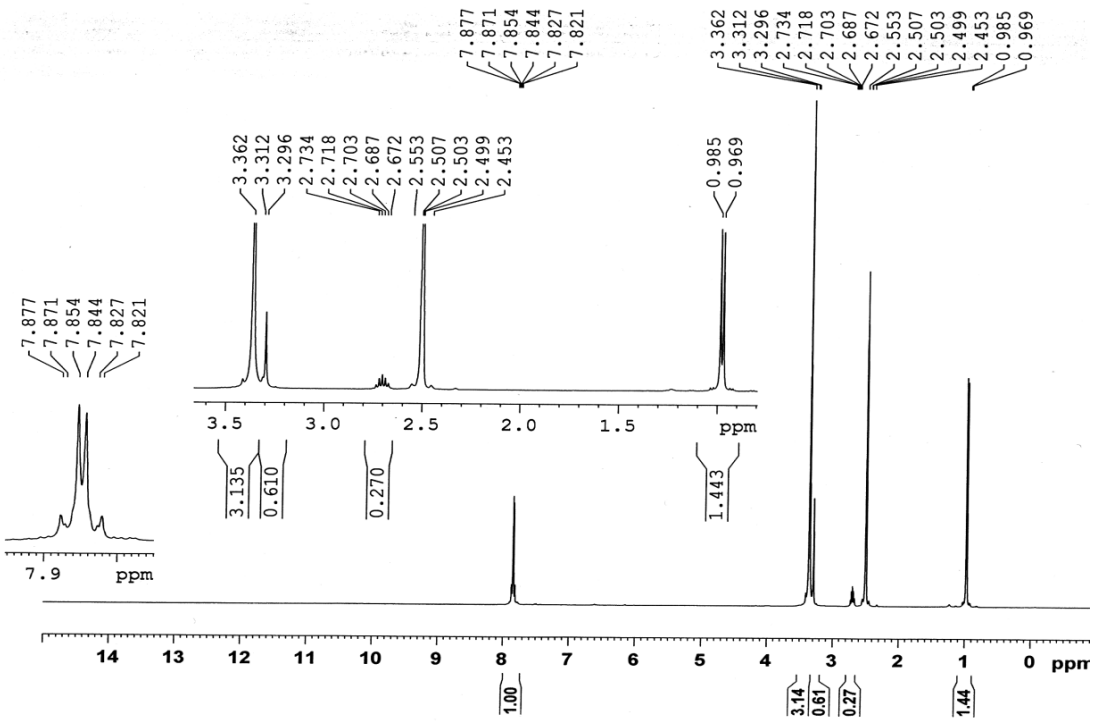

Annexure 14. ^{1}H NMR spectrum of L^{2} DMSO-d_{6}.

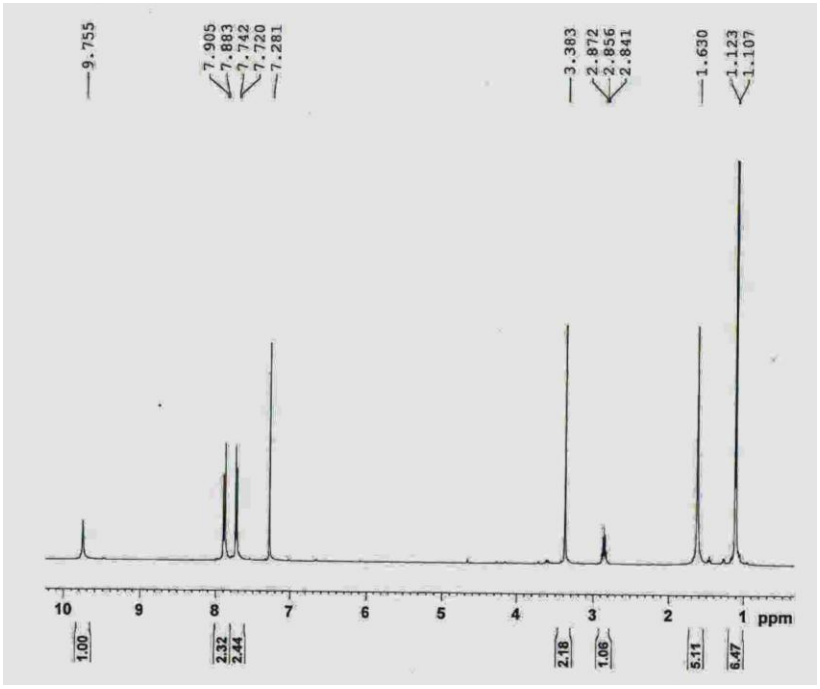

Annexure 15. ^{1}H NMR spectrum of L^{2} in $CDCl_{3}$.

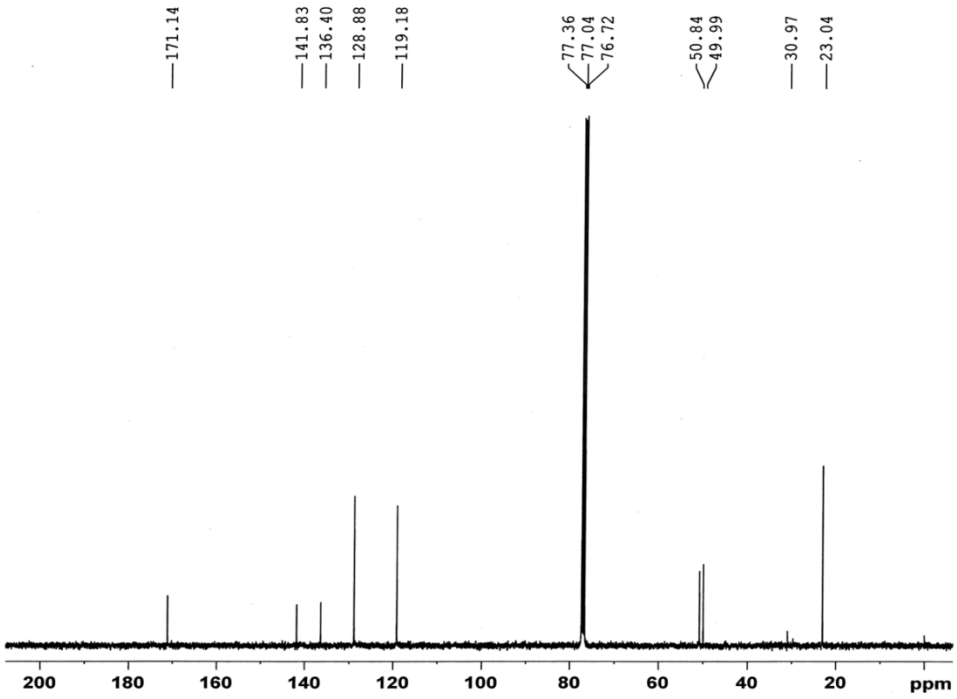

Annexure 16. ^{13}C NMR spectrum of L^2 in DMSO-d_6.

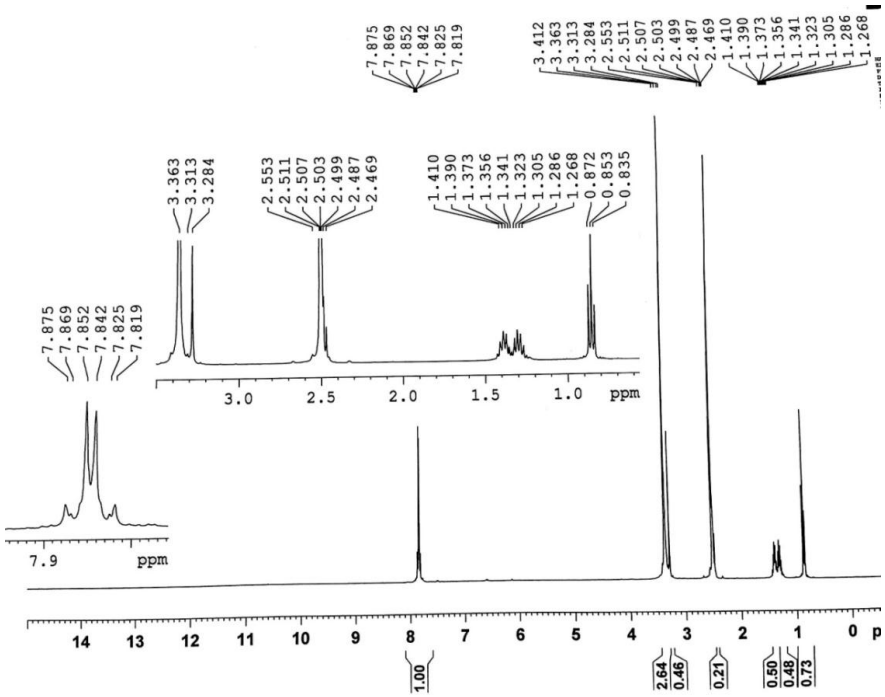

Annexure 17. ^{1}H NMR spectrum of L^3 in DMSO-d_6.

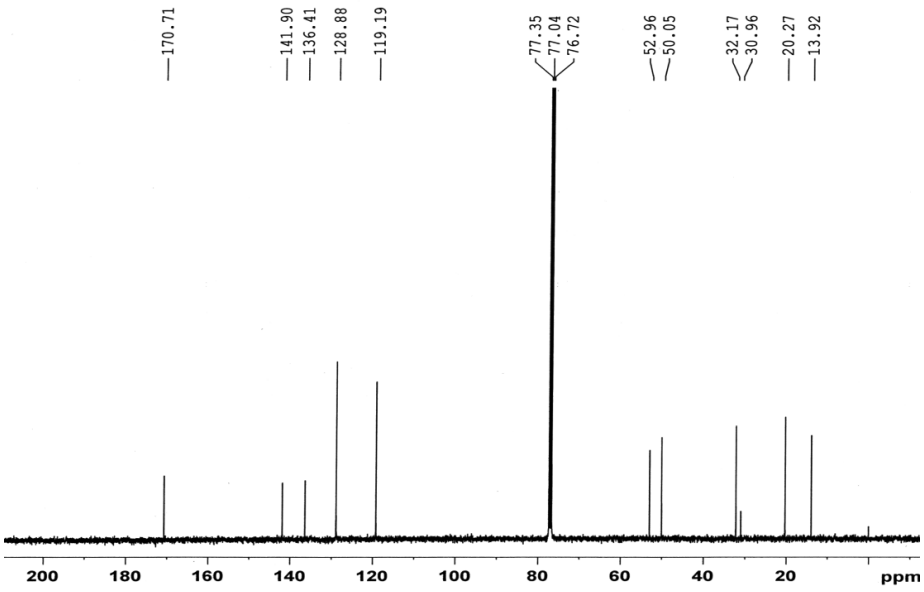

Annexure 18. ^{13}C NMR spectrum of L^3 in DMSO-d_6.

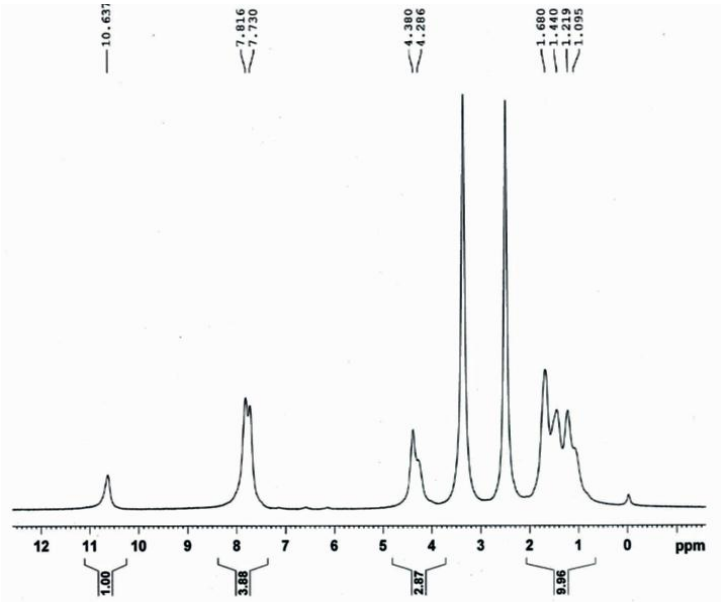

Annexure 19. ^{1}H NMR spectrum of **1a** in DMSO-d6.

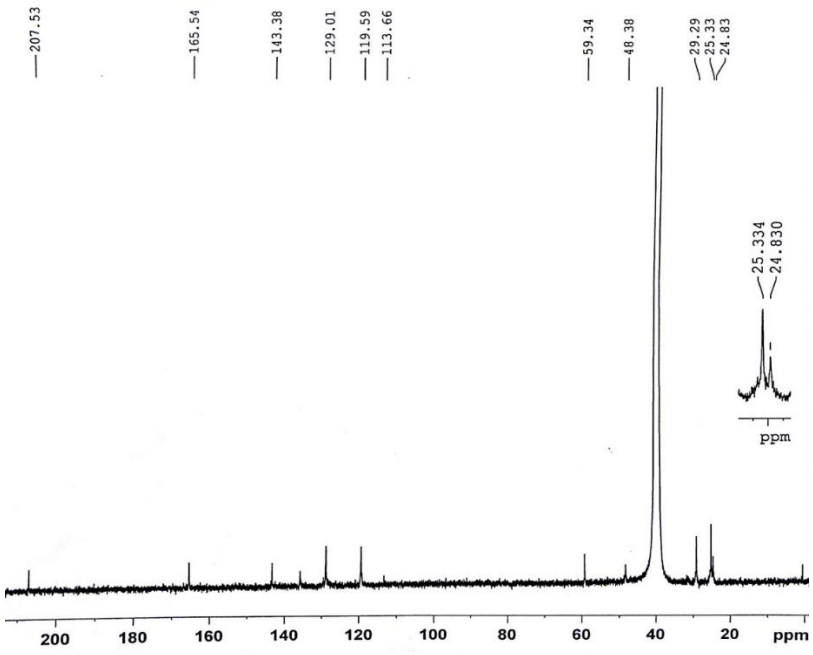

Annexure 20. ^{13}CNMR spectrum of **1a** in DMSO-d6.

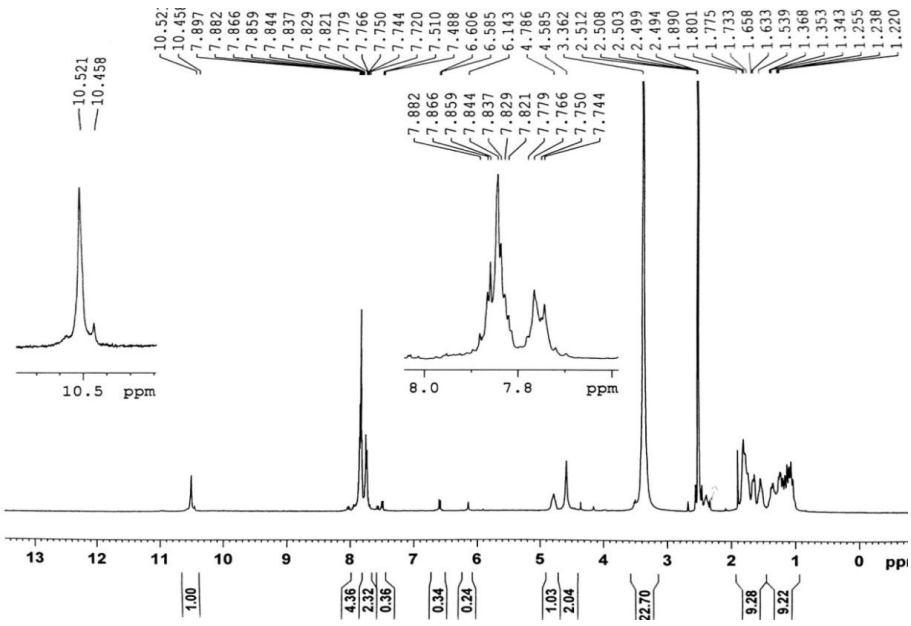

Annexure 21.^{1}H NMR spectrum of 1c in DMSO-d6.

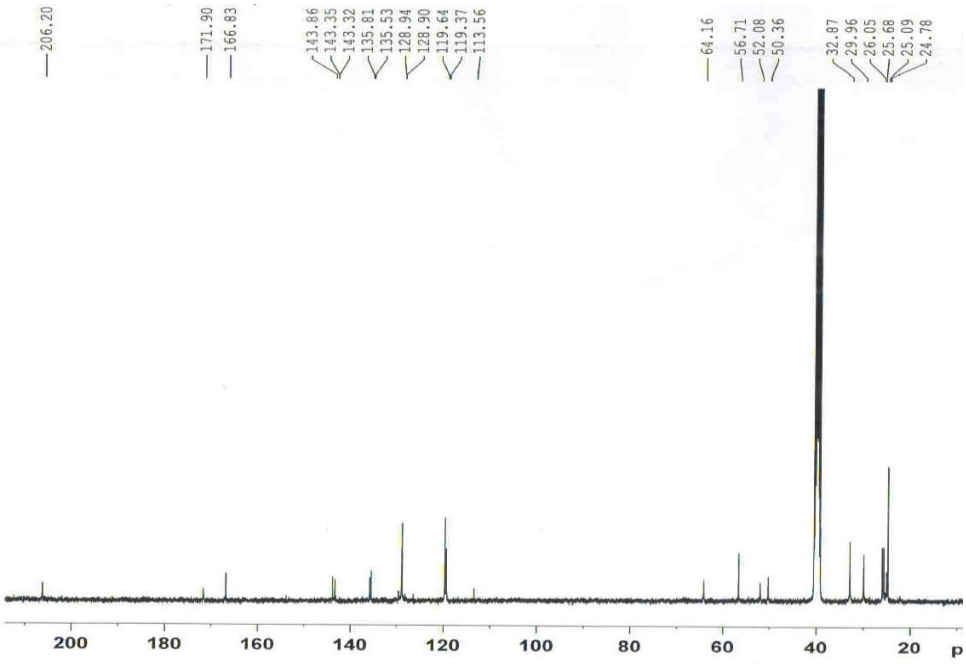

Annexure 22. ^{13}C NMR spectrum of 1c in DMSO-d6.

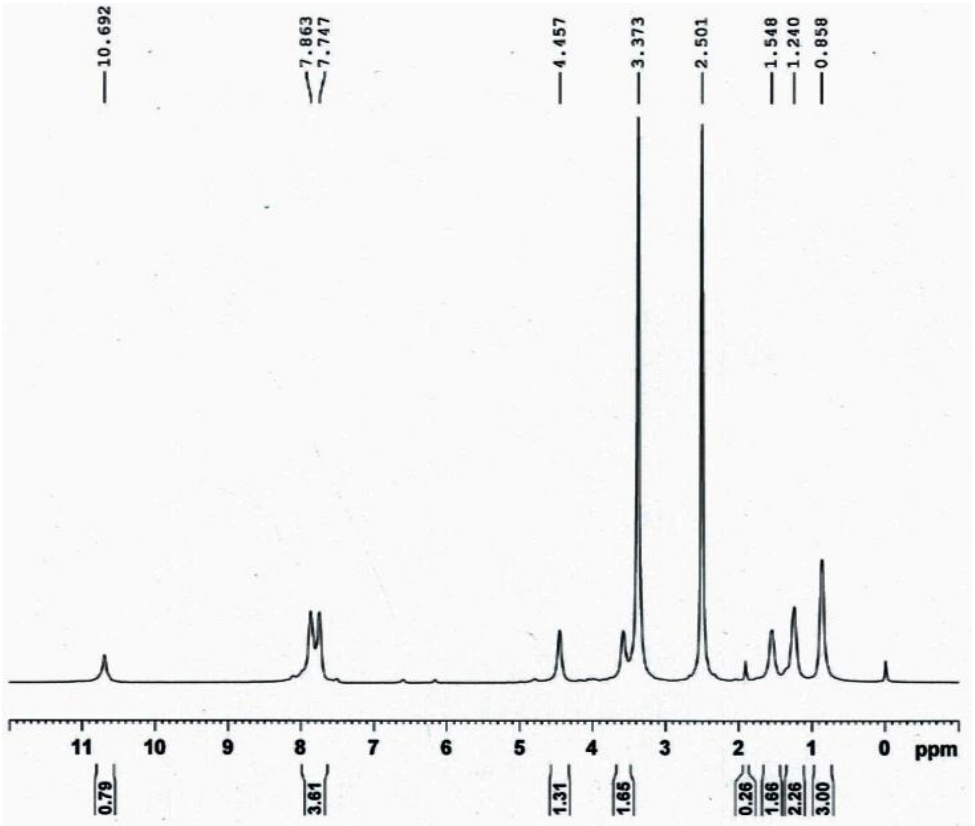

Annexure 23. ^{1}H NMR spectrum of 2**a** in DMSO-d6

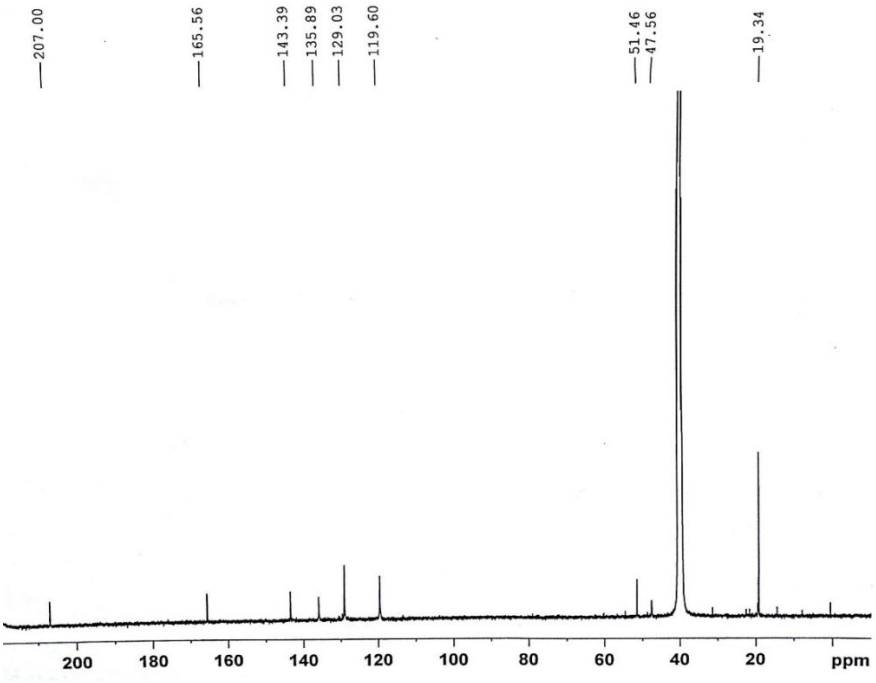

Annexure 24. ^{13}C NMR spectrum of 2**a** in DMSO-d6

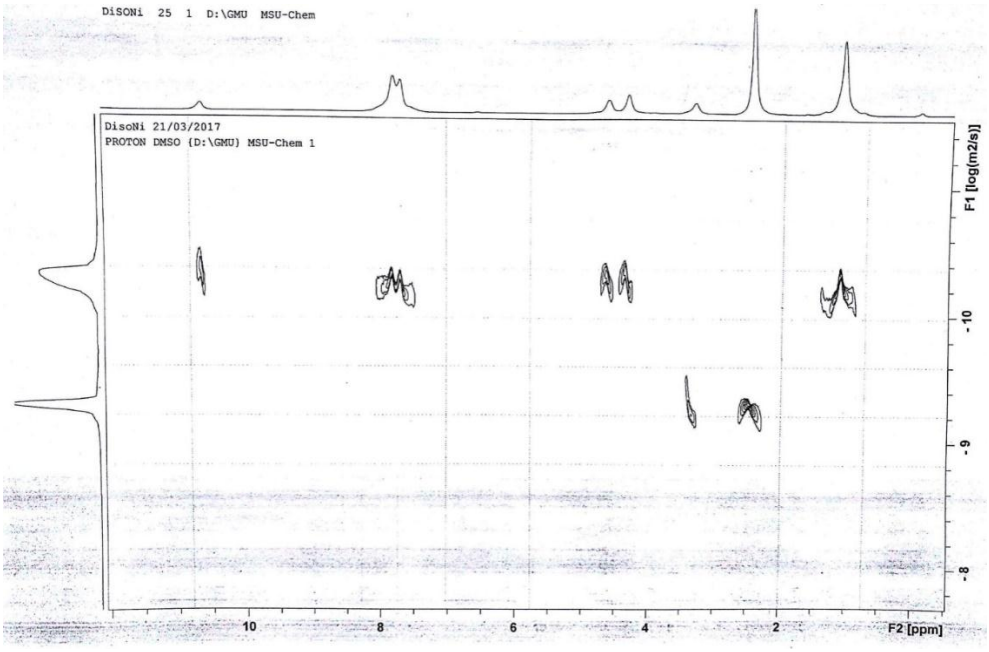

Annexure 25. DOSY NMR spectrum of 2a.

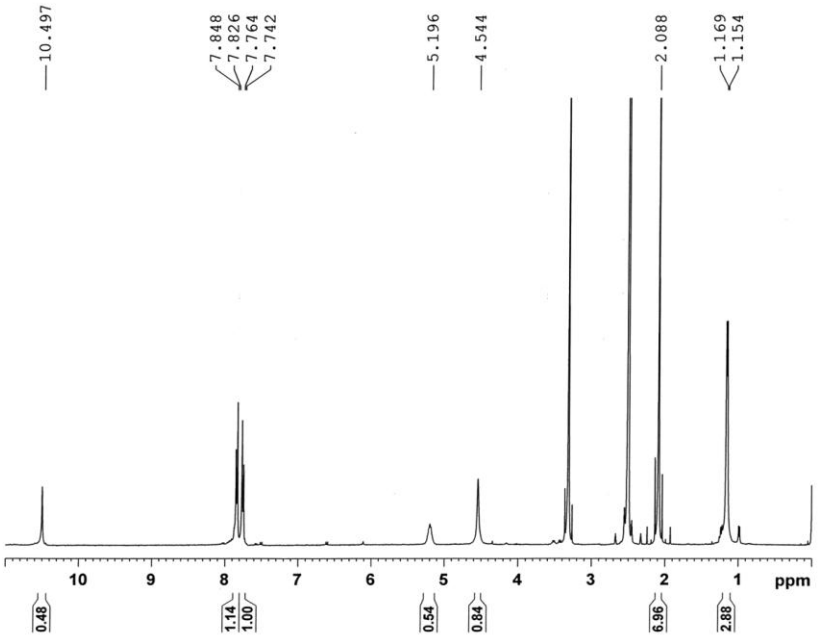

Annexure 26. ^{1}H NMR spectrum of 2c in DMSO-d6

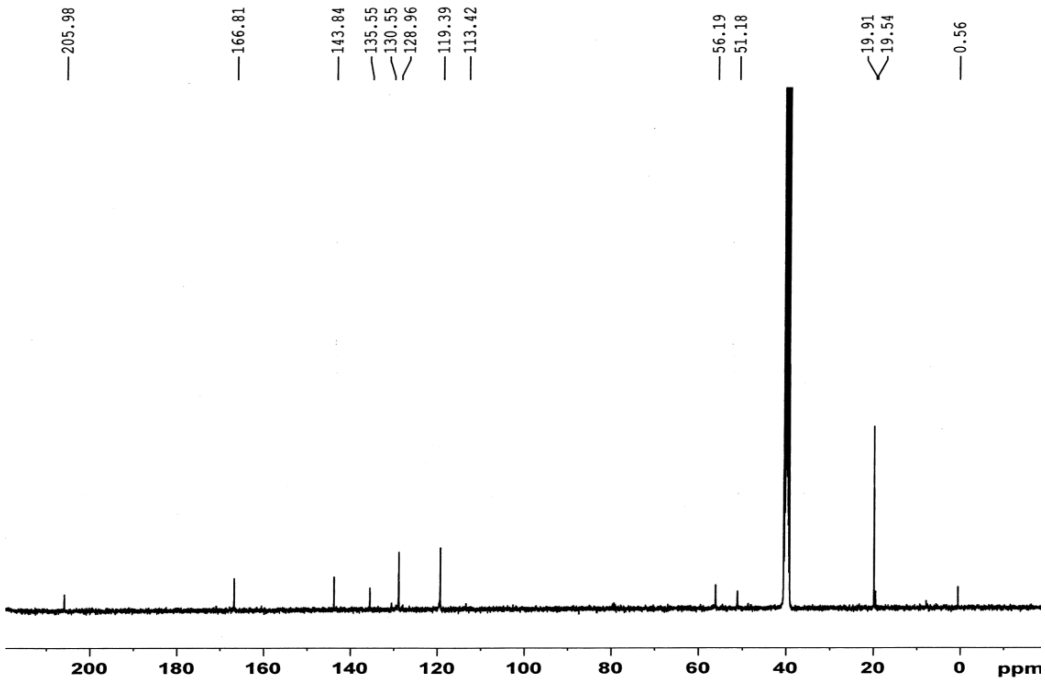

Annexure 27. ^{13}C NMR spectrum of 2c in DMSO-d6

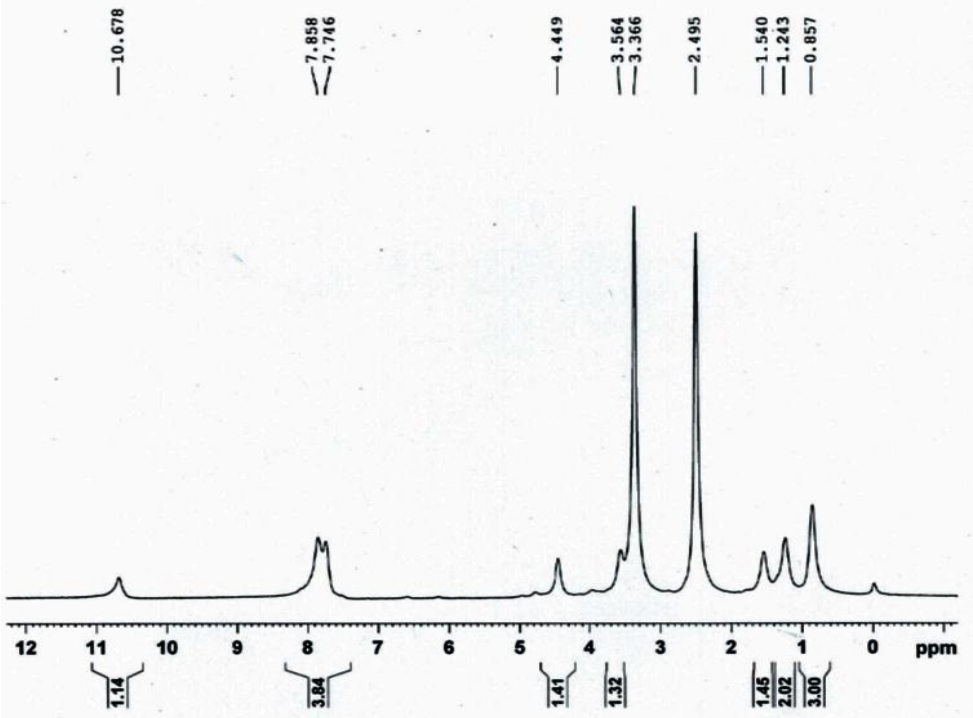

Annexure 28. ^{1}H NMR spectrum of 3a in DMSO-d6

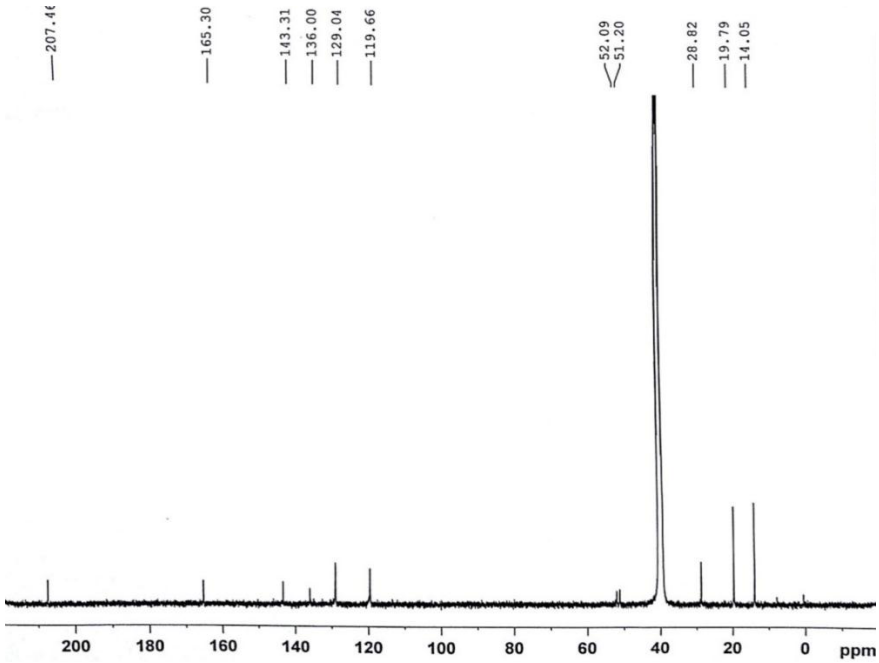

Annexure 29. ^{13}C NMR spectrum of 3a in DMSO-d6

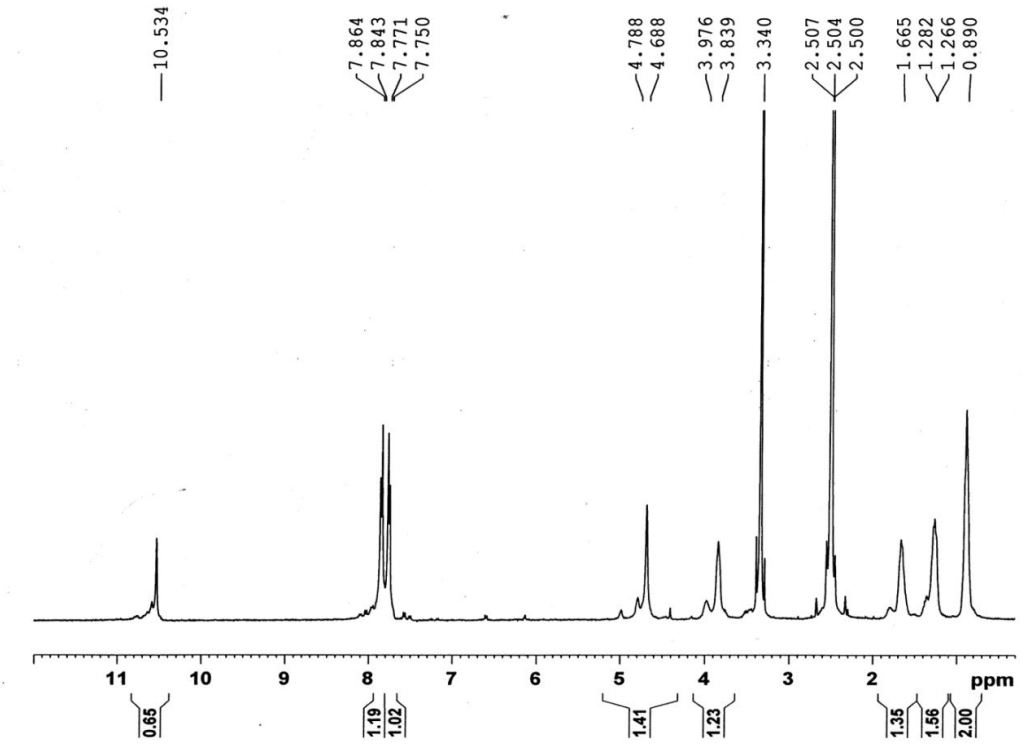

Annexure 30. ^{1}H NMR spectrum of 3c in DMSO-d6

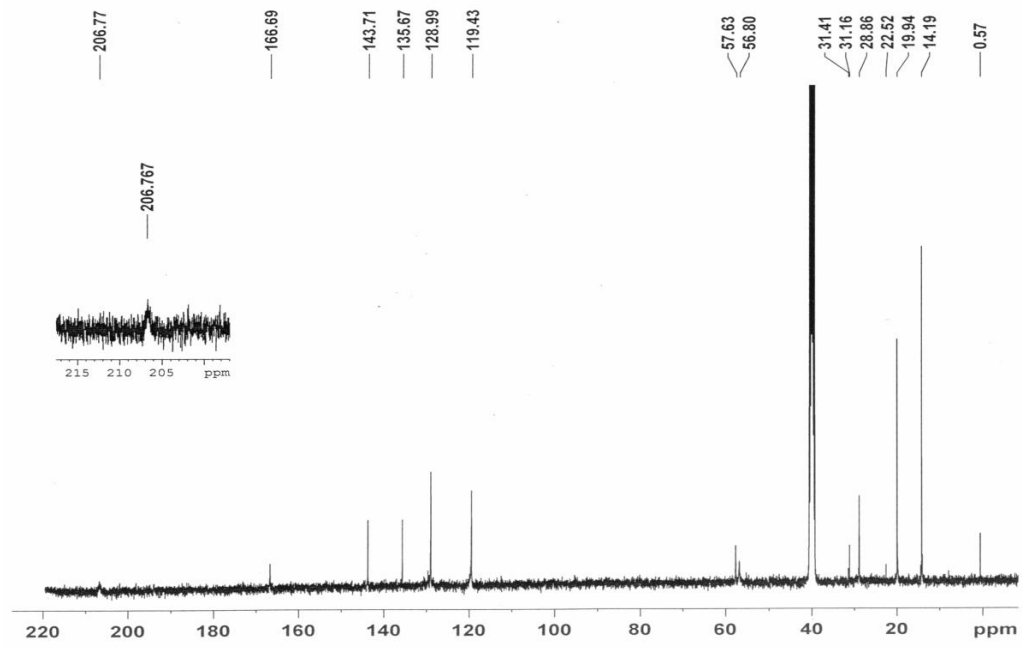

Annexure 31. ^{13}C NMR spectrum of 3c in DMSO-d^{6}

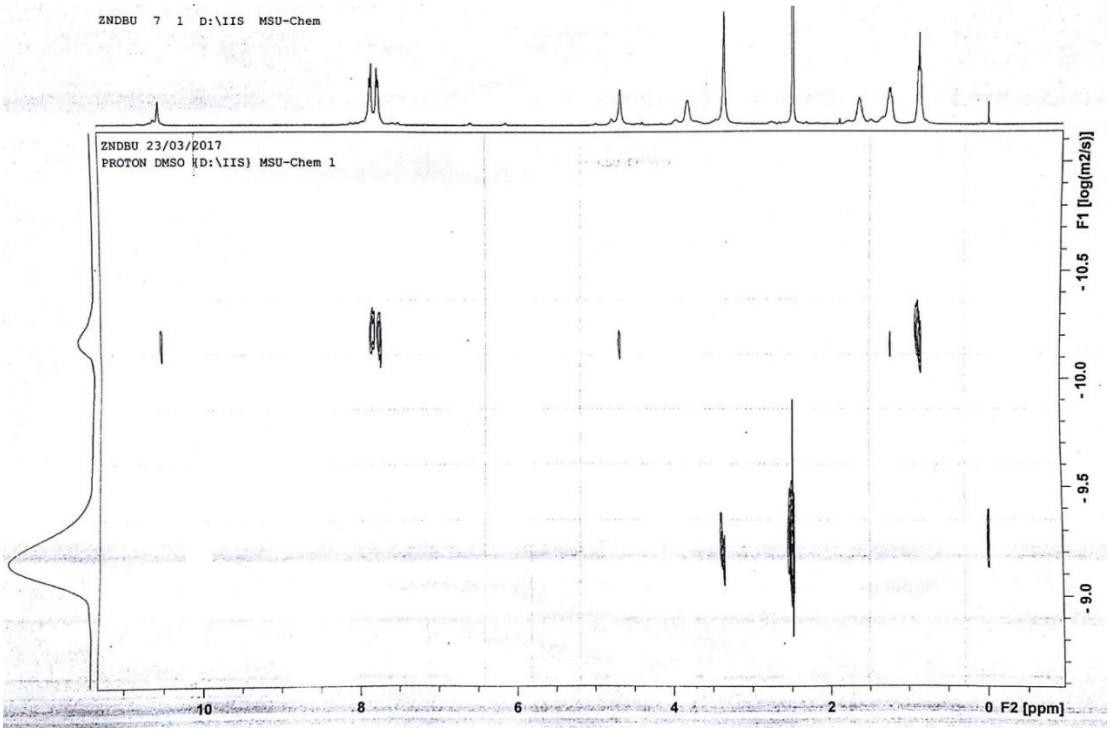

Annexure 32. DOSY NMR spectrum of 3c.

UV-visible absorption spectra:

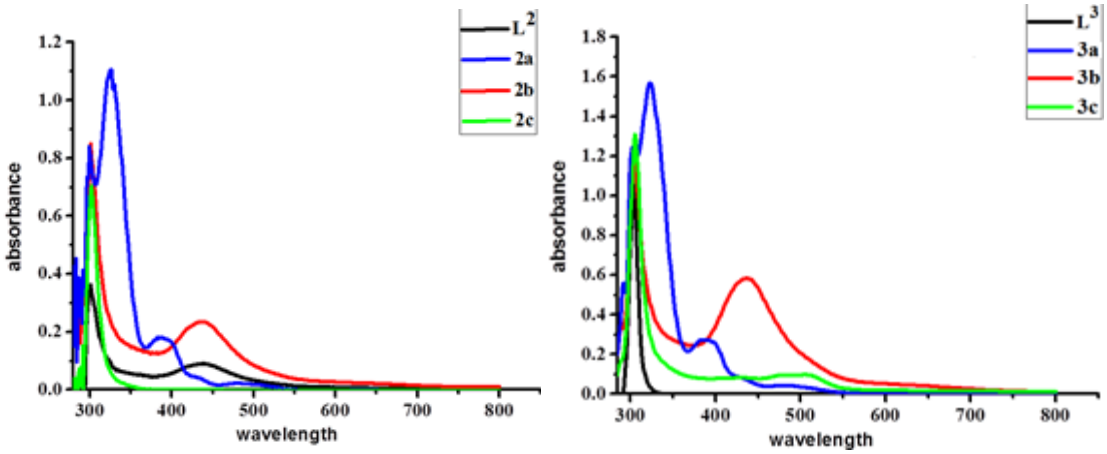

(a) (b)

Annexure 33.UV–visible absorption spectra (a) **L^2, 2a, 2b** and **2c**;(b) **L^3**, **3a, 3b** and **3c** in DMSO solution.

Emission spectra:

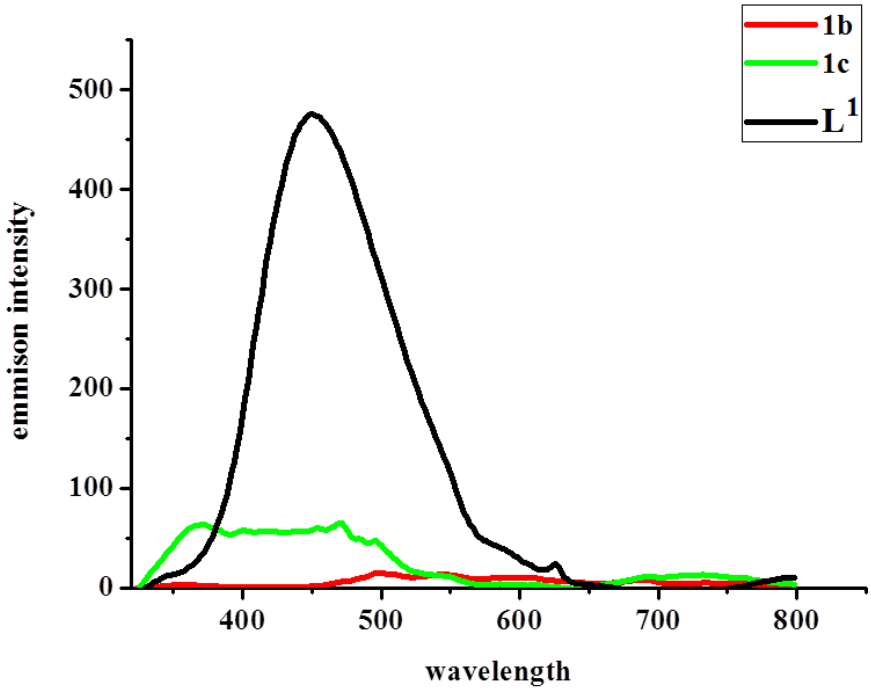

(a)

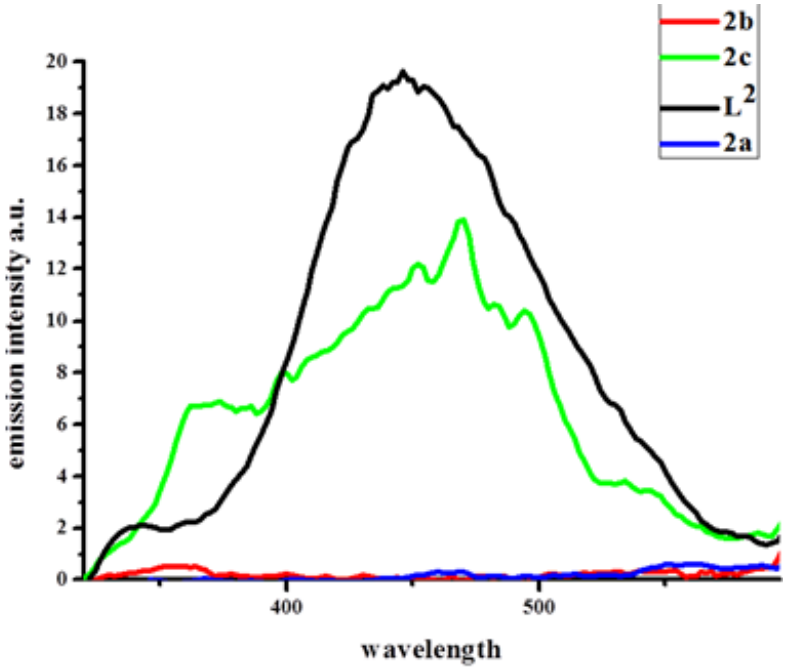

(b)

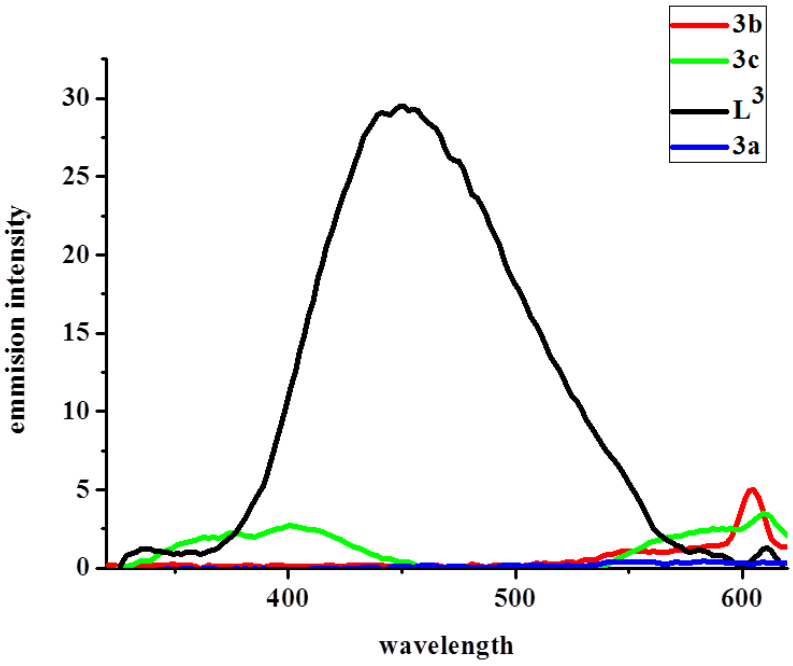

(c)

Annexure 34. Fluoresecenceemmission spectra of (a) $\mathbf{L^1}$ @ λ_{ex}= 309 nm, **1b** @ λ_{ex}= 304and **1c** @ λ_{ex}= 305 nm;(b) $\mathbf{L^2}$ @ λ_{ex}= 300 nm**,** **2a** @ λ_{ex}= 299 nm**,** **2b** @ λ_{ex}= 301 nm and **2c** @ λ_{ex}= 301 nm;(b) $\mathbf{L^3}$ @ λ_{ex}= 304 nm, **3a** @ λ_{ex}= 302 nm**,** **3b** @ λ_{ex}= 303 nmand **3c** @ λ_{ex}= 305 nmin DMSO solution.

2.6.2. Thermogravimetric studies

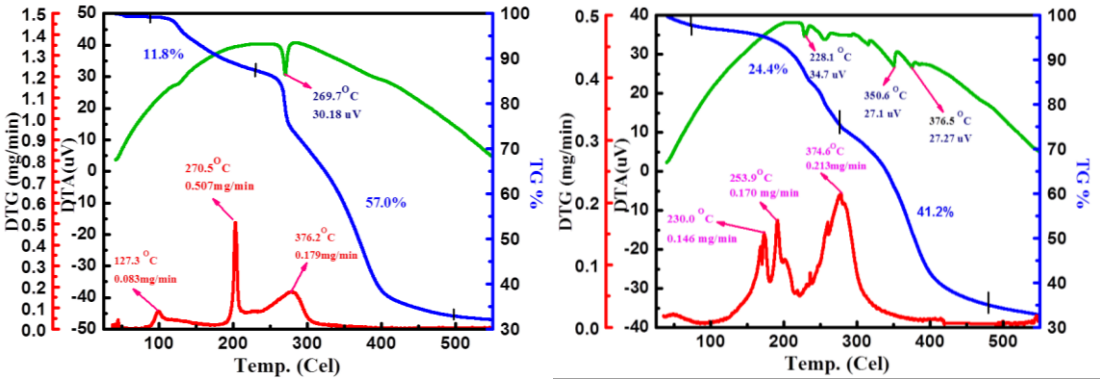

Compound 1a **Compound 1b**

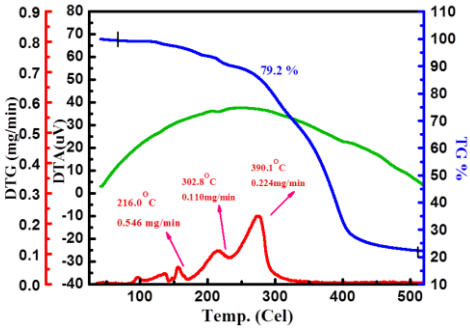

Compound 1c

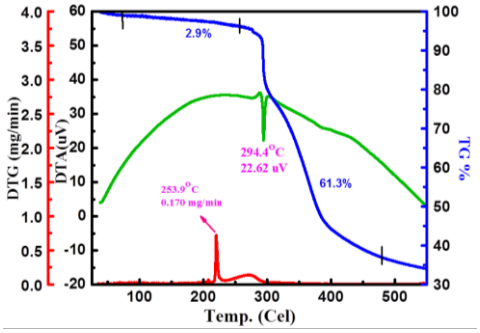

Compound 2a

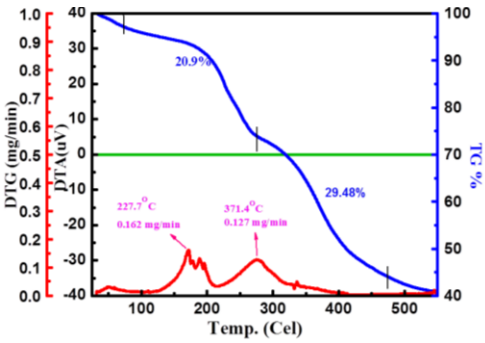

Compound-2b

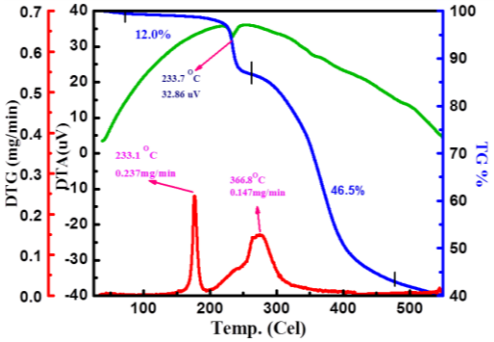

Compound-2c

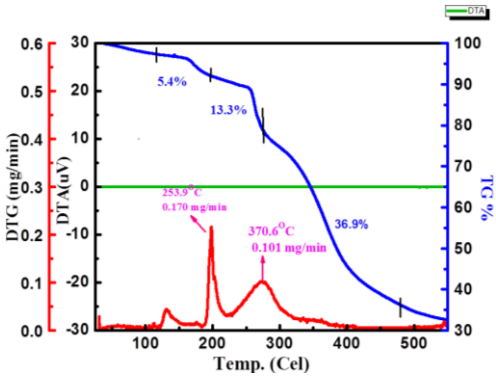

Compound- 3a

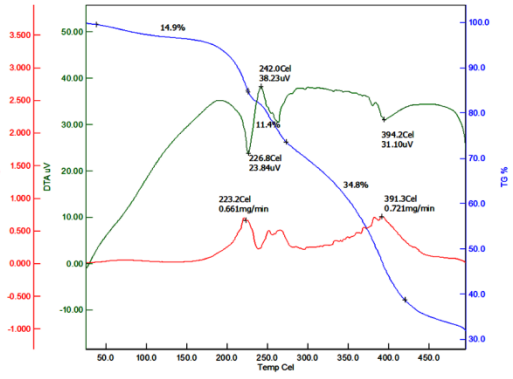

Compound- 3b

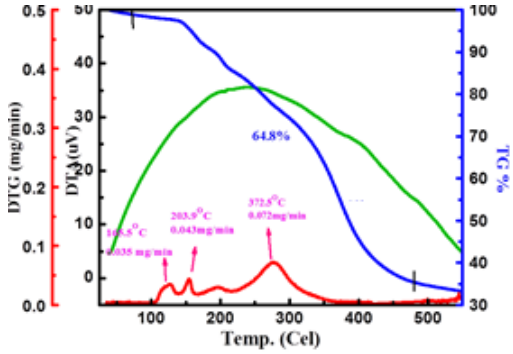

Compound-3c

Annexure 35. TGA/DTA plotsmetallomacrocyclic compounds.

Chapter 2

This part of work has been published in:

Pillai, V, Kadu, R, Buch, L, Singh, V. K, Derivatives of Dapsone (dap): Synthesis and Study on In Vitro Cytotoxic Activity and DNA Laddering against Hep G2 and C6 Human Cancer Cell Lines. ChemistrySelect **2017**, *2*, 4382-4391.

The additional supporting Information related to this chapter is provided in the CD as follows.

Chapter 2

1. NMR Spectra: **Figure 1.**
2. IR Spectra: **Figure 1-10**
3. Thermogravimetric analysis: **Table 1**
4. Geometry Optimization: **Table 2-5**
5. In vitro cytotoxic study: **Table 6-9** and **Figures 11-14**